國立臺灣大學理學院物理學研究所
碩士論文
Department of Physics
College of Science
National Taiwan University
Master Thesis

挑戰廣義相對論在極端尺度下的非線性效應
Confronting General Relativistic Nonlinearities in Macroscopic and Microscopic Universes

蔣序文
Chiang Hsu-Wen

指導教授：陳丕燊 博士
Advisor: Pisin Chen, Ph.D.

中華民國 壹零伍 年 陸 月
June, 2016

doi:10.6342/NTU201603461

doi:10.6342/NTU201603461

Acknowledgments

First, I would like to thank my advisor Prof. Pisin Chen, who spent countless hours on our weekly progress meetings and guided us through this amazing journey of physics study. I would also want to mention that if it were not for his wonderful lectures of cosmology, I would have been in other fields and may not have chances to involve in so many projects and met so many people in the group.

I'm deeply grateful to my collaborators Yao-Chieh Hu, Fabien Nugier, and Antonio Enea Romano. For Antonio Enea Romano, I appreciate your teaching of MATHEMATICA™ and also deeper and more complex parts of general relativity. I also thank your patience since I was still in the junior year of undergraduate when I started my first project. For Yao-Chieh Hu, I am glad that you also graduate this year. For Fabien Nugier, our weekly discussions have been very fruitful.

I also appreciate useful discussions with Prof. Ron Adler, Prof. Abhay Ashtekar, Prof. Yeong-Chuan Kao and Dr. Peter Scicluna. Without you, some parts of this thesis may never be finished.

I would want to thank for your aspiring lectures and your will to share great knowledges in physics, to Prof. Pao-Ti Chang, Prof. Yih-Yuh Chen, Prof. Jiunn-Wei Chen, Prof. Shou-Huang Dai, Prof. Xiao-Gang He, Prof. Pei-Ming Ho, Prof. Keisuke Izumi, Prof. Yeong-Chuan Kao, Prof. Jiwoo Nam, and Prof. Mu Tao Wang.

Your enthusiasm, your classmate-ship, your discussions on physics just give me the most incredible study experience of my life, to Che-Yu Chen, Chien-Ting Chen, Chun-Yen Chen, Hsiao-Yi Chen, Po-Ta Chen, Yi-Chun Chen, Chia-Wei Hsing, Ke-Chih Lin, Yu-Hsiang Lin, Hua-Ciao Lyu, Yen Chin Ong, and Che-Min Shen.

Finally, I just want to thank two more people. When I was 8 years old I went to Taipei astronomical museum for the first time and became obsessed with black holes, main sequence stars, etc. My father and mother then took me to the museum almost weekly. They support me through all these years. So for Jack and Lisa, thank you.

This thesis is supported by National Center for Theoretical Sciences (NCTS) of Taiwan, Ministry of Science and Technology (MOST) of Taiwan, and the Leung Center for Cosmology and Particle Astrophysics (LeCosPA) of National Taiwan University.

doi:10.6342/NTU201603461

中文摘要

本碩士論文依據作者過去發表的文章[2, 9]分成兩大部分。

首先，我們認爲與以往的微擾計算結果相反，廣義相對論的非線性效應會讓宇宙小尺度的不均勻性足以改變超新星亮度距離與紅移的關係，使得從超新星推得的哈伯常數與從宇宙微波背景輻射得來的數值不同。我們計算並顯示已知的3.4個標準差的差距確實可以用一個約莫三億秒差距大小的空洞來解釋，同時該空洞與亮物質密度觀測數據暗示可能存在的空洞大小位置相符。

然後在第二部分，我們基於廣義相對論中常常出現的旋量變數，透過將弦世界面理論對稱轉變爲旋量對稱來建立一個新形式的時空量子化。由於是從幾種常見的重力理論共有的特性出發，我們相信此理論可以將如量子迴圈重力理論與超弦理論等熱門理論連結起來。我們也推導了廣義測不準原理並顯示理論具有全相性。由於時空被量子化，世界線會變得比較模糊。我們計算了模糊的程度，並顯示即便是在宇宙學尺度下也極難測量到該現象。因此我們無需擔心這個時空量子化理論會與任何宇宙觀測結果相衝突。

doi:10.6342/NTU201603461

Abstract

The whole thesis is divided into two parts, each of which is based on papers[2, 9] published before.

First, we suggest that contrary to the usual perturbation result, the increasingly severe Hubble parameter tension between observations by utilizing low-redshift supernovae luminosity distance and the cosmological microwave background can be explained away by considering the nonlinear effect of the local inhomogeneity. We also compare the density profile from galaxy survey to what we obtained from the assumption that the tension of Hubble parameter comes solely from the local inhomogeneity, and find that they agree with each other.

Second, we introduce a new type of spacetime quantization based on the spinorial description suggested by loop quantum gravity. Specifically, we build our theory on a string theory inspired Spin(3, 1) worldsheet action. Because of its connection with quantum gravity theories, our proposal may in principle link back to string theory, connect to loop quantum gravity where SU(2) is suggested as the fundamental symmetry, or serve as a Lorentzian spin network. We derive the generalized uncertainty principle and demonstrate the holographic nature of our theory. Due to the quantization of spacetime, geodesics in our theory are fuzzy, but the fuzziness is shown to be much below conceivable astrophysical bounds, which makes our theory safe from deleterious effects.

doi:10.6342/NTU201603461

doi:10.6342/NTU201603461

Contents

Acknowledgments **i**

中文摘要 **iii**

Abstract **v**

Contents **vii**

List of Figures **ix**

List of Tables **xi**

1 Introduction **1**

1.1 Standard Model of Cosmology 2

2 Distance Measurement in GR **5**

2.1 Anchors and the Cosmic Ladders 6

2.2 Tension on H_0 between Supernovae and CMB Measurements 7

3 Inhomogeneity of the Universe **9**

4 Data Analysis **13**

4.1 Linear Regression and χ^2 Analysis 13

4.2 Monte Carlo + Local Optimization 15

5 Easing H_0 Tension by Invoking Local Inhomogeneity **19**

5.1 Geodesic Equation and the Initial Condition 19

5.2 Mapping D_L back to Density Contrast 22

5.3 Result 24

6 Quantization of Spacetime **31**

6.1 Dimensional Reduction of Momentum Space 32

6.2 Angular Momentum Space and $U(\mathfrak{su}(2))$ algebra 33

6.3 Adler's Spinorial Spacetime 34

7 Spinorial Spacetime **35**

7.1 Reinterpretation, Reformulation and Correction to Adler's Proposal . . . 35

7.2 Obtainbing Action Through Fermionization 39

7.3 Composite and Holographic Nature of the Spacetime 42

7.4 Generalized Uncertainty Principle 44

doi:10.6342/NTU201603461

7.5 Smearing Effect 45

8 Conclusion and Future Work **47**

8.1 Macroscopic Universe 47

8.2 Microscopic Universe 47

Appendices **49**

Bibliography **51**

doi:10.6342/NTU201603461

List of Figures

4.1 Work-flow of the fitting procedure. Δm stands for difference between observed magnitude and the predicted value from the FRW model with PLANCK 2016 parameters. Here LR stands for lineara regression, NL for nonlinear, param. for parameters, and CL for confidence level. The double arrow consists of n copies of flows, each of which has a different data point deleted. The idea of inversion will be introduced in the next chapter. 17

5.1 This plot shows the sky map of all SNe and cepheids in our dataset. Three fields are specified in Keenan's work [7] as the three regions with density contrast data. Our targets of interest are field 1 and field 3 which contain enough data points to fit the luminosity distance curve. For the sake of clarity we will keep using the same color for field 1 and field 3 as [7] later on. 25

5.2 This plot shows the 68% confidence band of the field 3 Δm fit, along with the data points in this region. The deleted data points are in a darker color. The dashed curves are the 68% confidence band envelop and the vanilla curve is the best fit. The fitting model is chosen to be 5 functions of the form $\Phi(r) = r^3$ according to the dimensional argument of the polyharmonic spline interpolation method. The gray curve is the result from Riess 2016 [3]. 26

5.3 This plot shows the 68% confidence band of the field 1 Δm fit, along with the data points in this region. The deleted data points are in a darker color. The dashed curves are the 68% confidence band envelop and the vanilla curve is the best fit. The fitting model is chosen to be a simple constant shift. The gray curve is the result from Riess 2016 [3]. 27

doi:10.6342/NTU201603461

5.4 This plot shows the 68% confidence band of the inverted density contrast of the field 3, with $K_0 = -0.1$. Clearly we can see a ∼68% significant 10% under-dense around $z = 0.02$ to 0.08 or $100 \sim 400$ Mpc. One can directly compare this plot to Keenan's using conversion $d(Mpc) = H_0^{-1}z = 4400\,z\,Mpc$. One important feature in Keenan's result is the overdense region at around $z = 0.1$, and as we can see such feature is in the 68% confidence band of our result. The gray curve is the inverted density contrast of the FRW model with parameters from Riess 2016 [3]. . 28

5.5 This plot shows the 68% confidence band of the inverted density contrast of the field 1, with $K_0 = -0.1$. Clearly we can see a ∼95% significant 10% under-dense everywhere. One can directly compare this plot to Keenan's using conversion $d(Mpc) = H_0^{-1}z = 4400\,z\,Mpc$, and find that the two agree with each other pretty well. The gray curve is the inverted density contrast of the FRW model with parameters from Riess 2016 [3]. . 29

5.6 This plot shows the inverted density contrast of the best fit in the field 3, under different K_0. The blue, green, red curves correspond to $K_0 = -0.1$, 0, and 0.1 respectively. 30

doi:10.6342/NTU201603461

List of Tables

7.1 A commutativity table showing possible ways of labelling Hilbert space. For elements T_{mn} inside the table, “O” means m-th basis commutes with n-th basis, and “X” means non-commutativity. Here all vectors are along spatial eigen-direction $n^i = \langle \Delta X^i \rangle$, and $\Delta\vec{X} = n_i \Delta X^i$ is the spatial interval, $\Delta V_3 = \Delta X^1 \Delta X^2 \Delta X^3$ is the time-like 3-volume, $\Delta\vec{V} = -n_i \epsilon^i_{jk} \Delta X^0 \Delta X^j \Delta X^k$ is the spatial 3-volume, Δt is the time difference, Δs^2 is the proper distance square, $\Delta\vec{A} = n_i \epsilon^i_{jk} \Delta X^j \Delta X^k$ is the spatial area, $\Delta\vec{A}_t = n_i \Delta X^0 \Delta X^i$ is the time-like area, and $\Delta V_4 = \Delta X^0 \Delta X^1 \Delta X^2 \Delta X^3$ is the 4-volume. Notice that actually $\vec{V}$ can always be described by products of two non-trivial quantum numbers in the system. 37

doi:10.6342/NTU201603461

Chapter 1

Introduction

General relativity (GR) has been hailed as one of the most elegant and successful theories in the history of physics. It has passed numerous experimental tests, and also laid the foundation of the standard model of cosmology. But however marvellous it may be there are still pit holes that puzzle physicists generation after generation. The most bizarre feature of GR is probably its non-linearity. In theories that are linear, e.g. Maxwell theory, doubling the charge density would not result in anything special, at least classically. However, in GR if one throws too much mass to the same location, a black hole may be created, and the characteristics of the system changes completely around the event horizon.

On the other hand, in the standard model (SM) of cosmology the universe is considered homogeneous and isotropic at the large scale limit, and small structures like superclusters or galaxies are just perturbations on top of that, which tweak the observation slightly at higher orders. This statement seems in contradiction with the non-linearity of GR, and a natural question thus arises. Are these inhomogeneities really incapable of modifying cosmological observations significantly? We suggest that in fact there are evidences of drastic deviation from SM of cosmology in local Hubble parameter (H_0) measurements using supernovae (SNe) as standard candles. In this thesis we point out that the tension between H_0 measurements based on cosmological microwave background (CMB) and SNe can be explained away by positing a void around 300 mega-parsec (Mpc) wide. We develop a technique that can convert the luminosity distance (D_L) measurement back to the density contrast profile, and show that indeed it is to some degrees similar to what was observed through galaxy surveys [7].

The non-linearity of GR also becomes the blocking stone when one tries to quantize it. A näive perturbation series expansion would result in non-renormalizable divergences simply because every energy, including gravitational energy, gravitates. One thus concludes that additional features must be added. For the past fifty years physicists have

doi:10.6342/NTU201603461

introduced various features, including supersymmetry, higher dimensions, strings, and tetrads in the pursuing of a quantum theory of gravitation. Interestingly both loop quantum gravity (LQG) and superstring theory, the two most popular quantum gravity theories, exhibit a minimal distance, suggesting that the spacetime may be quantized. On the other hand, many formalisms, including Newman-Penrose formalism, Bondi-Metzner-Sachs symmetry on null infinity and loop quantum gravity, are based on the spinor description. We therefore construct a new spacetime quantization model based on spinorial variables, and show that it has many interesting properties.

For the sake of readability, IJK are for $SO(3,1)$ tangent bundle coordinate indices, $\mu\nu\lambda\rho$ for 4-d coordinate, ijk for 3-d coordinate, $\alpha\beta\gamma$ for 2-d coordinate, and $(i)(j)(k)$ for site numbers. Gamma matrices γ are defined according to the type of the indices (Minkowskian if unspecified). We also use natural units $c = \hbar = G = 1$, $\dot{a} = \frac{\partial a}{\partial t}$, $a_{,r} = \frac{\partial a}{\partial r}$, and the signature of g is chosen to be $(+,-,-,-)$.

1.1 Standard Model of Cosmology

As we mentioned in ch.1 the standard model of cosmology is built on an assumption that the universe is homogeneous and isotropic at the large scale limit. The metric corresponding to this assumption is the Friedmann–Robertson–Walker (FRW) metric

$$ds^2_{FRW} = dt^2 - a\left(t\right)^2 \left(\frac{1}{1-kr^2}dr^2 + r^2 d\Omega^2\right) , \tag{1.1}$$

where a is the scale factor that defines how the universe "expands" or "collapses" in the sense that every matter comoves as the universe expands or collapses, $d\Omega^2$ is the line element for unit 2-sphere, and k is the spatial curvature that determines the geometry of the 3-d space ($k = 1$ for sphere, $k = 0$ for flat plane and $k = -1$ for hyperbola). From CMB observations it has been known that $k \sim 0$, i.e., the universe is almost flat. The spatial curvature is very often confused with the spacetime curvature, but actually it only describes the curvature of space. So even in flat FRW universe the curvature, i.e. the matter density, does not vanish.

From Einstein Field Equation (EFE) one immediately obtains the Friedmann equations

$$H^2 = \frac{8\pi}{3}\rho - \frac{k}{a^2} + \frac{\Lambda}{3} , \tag{1.2}$$

$$\dot{H} = -\frac{4\pi}{3}\left(\rho + 3p\right) + \frac{\Lambda}{3} , \tag{1.3}$$

where $H = \dot{a}/a$ is the Hubble parameter, ρ is the matter density, p is the pressure, and Λ is the cosmological constant.

doi:10.6342/NTU201603461

Clearly without the cosmological constant the usual dust-like matter ($p = 0$) would results in a dynamical universe with a variable scale factor. Discovery of the Hubble's law proves that we are living in a dynamical universe, since further the astronomical object is faster it is moving away from us. This apparent universal retreating is called "redshift", and can be explained not by the Doppler effect but by the expansion of the universe that stretches the electromagnetic (EM) wave and reddens the light. Hubble's law can be expressed as

$$z \approx H_0 D \,, \tag{1.4}$$

where H_0 is the Hubble parameter of the present day, D is the distance, $z = \frac{a_0}{a} - 1$ is the redshift, and a_0 is the scale factor of the present day.

It may seem all fair given the observational fact, but one immediately realize that by winding back the clock, the universe is actually coming from an extremely dense and hot point with $a = 0$, i.e., the big bang. One of the most successful prediction of the cosmology is that there exist residual lights of this primordial hot gas, i.e., the cosmological microwave background (CMB). The observed temperature of 3K also sets $z_{CMB} = 1100$.

There is still a loophole in the entire argument. How can one side of CMB have the temperature as the other side of it? To answer this one needs to introduce the idea of inflation: a rapid expansion period before CMB which allows the causal connection between two ends of the sky. Naïvely the cosmological constant serves the role, but since we need to stop such a rapid expansion, what we need is some kind of dynamical cosmological constant.

The simplest realization is through a scalar field called inflaton. With a scalar field ϕ the Friedmann eqs. become

$$H^2 = \frac{8\pi}{3}\left(\frac{1}{2}\dot{\phi}^2 + V(\phi)\right) \,, \tag{1.5}$$

$$\dot{H} = -4\pi\dot{\phi}^2 \,. \tag{1.6}$$

To make sure the inflaton is similar to the cosmological constant, we introduce the idea of slow roll:

$$H^2 = \frac{1}{3}\left(8\pi V(\phi) - \dot{H}\right) \approx \frac{8\pi}{3} V(\phi) \,, \tag{1.7}$$

which immediately leads to

$$\epsilon = \frac{1}{16\pi}\left(\frac{V'}{V}\right)^2 \ll 1 \,, \tag{1.8}$$

$$\eta = \frac{1}{8\pi}\frac{V''}{V} \ll 1 \,. \tag{1.9}$$

doi:10.6342/NTU201603461

ϵ and η are the slow roll parameters that characterize the inflation. Given a roughly constant acceleration, there is a horizon at H^{-1} that has a temperature of $H/2\pi$, which then perturbs the inflaton field. The fluctuation of the inflation field then seeds the inhomogeneity that grows into large scale structures and CMB anisotropies. In SM of cosmology, the impact on the observations due to the inhomogeneity has been studied thoroughly up to first order. However as we argued at the beginning of this chapter, the non-linearity of GR creeps in as the perturbation grows into filaments and voids. In the following chapters we will explain how such effect would modify one of the most important measurements, the distance measurement in an unexpected way.

doi:10.6342/NTU201603461

Chapter 2

Distance Measurement in GR

In usual experiments, using a ruler is the easiest way to measure the distance. However this method is not applicable at the astronomical scale. To measure such great distance one must rely on something that can travel through the vacuum, e.g. EM wave. Using Earth's orbit as the ruler, parallax can measure distances to lots of astronomical objects that are within our own Milky Way (MW). This is also how one defines the "parsec" (pc): an object having parallax movement of 1 arcsecond is 1pc away.

For objects that are even further from us, parallax is not so useful as the intrinsic scale of the method is the circular orbit of Earth. One therefore must rely on non-geometrical methods. The simplest way would be the standard candle. Given a candle with known luminosity at a certain distance, one can easily get the distance of that candle by

$$D_L = \sqrt{\frac{L_0}{L}} D_0 \,, \tag{2.1}$$

where L_0 is the known luminosity at distance D_0, L is the measured luminosity and D_L is the luminosity distance. There are several types of objects with almost constant energy outputs regardless of where or how old they are, and astronomers use these so called standard candles of cosmology to determine the distance. Cepheids and SNe are probably the most famous two as both of them are very bright, have very accurately measured energy outputs, and the light curves are well-explained.

The distances obtained in three different ways mentioned above are exactly the same in Minkowski spacetime. But in curved spacetime the equivalence is not guaranteed. In flat FRW universe one can easily obtained the three distances as following:

$$D_C(z) = \int_0^z \frac{dz'}{H(z')} \,, \quad D_A(z) = \frac{D_C(z)}{1+z} \,, \quad D_L(z) = (1+z)\, D_C(z) \;. \tag{2.2}$$

Here the comoving distance $D_C(z)$ describes the current distance of an object of redshift z measured by a ruler, the angular diameter distance $D_A(z)$ describes the relation between angular motion and transverse motion, and D_L is precisely the luminosity distance measured using standard candle.

To certain degree the redshift is the ultimate distance measure tool once H_0 and the constants in eq. (1.2) are determined. However as we can see the relation between three distances depends on the geometry of the spacetime, or the matter distribution itself. Therefore it opens the possibility that the inhomogeneity may alter these relations and thus induce some effects on the distance measurements, and thus on the measurement of H_0.

2.1 Anchors and the Cosmic Ladders

As we mentioned in the last section, to obtain the luminosity distance one needs a standard candle with a fully explained light curve and an accurately measured energy output. But in reality one cannot really measure the total energy output as these standard candles are still astronomical objects. What one really know is just their magnitude

$$m = -2.5 \log_{10} L\,, \tag{2.3}$$

where the luminosity L is in a predefined unit. Therefore some specific objects with distances measured in other ways are used to determine the so called absolute magnitude M (expected magnitude of the object at 10pc). These special objects are called anchors.

For example, MW cepheids are the anchors to determine the absolute magnitude of the cepheids since they are close enough to use parallax to determine the distance. Cepheids in turn determine the absolute magnitude of SNe by comparing SNe to cepheids within their host galaxies. SNe then determine the relation between redshift and distance by determining H_0 and constants in eq. (1.2). This series of anchoring is called cosmic distance ladder. Clearly the accuracy of this long chain of measurements could easily be compromised by unexpected contaminations coming from local inhomogeneities. Later on we will analyse one specific part of the ladder, the determination of the SNe absolute magnitude and H_0.

Another way to measure H_0 is through the observation of CMB. The sound horizon of baryons during CMB era can be fully determined by cosmological models fitted using CMB data. This sound horizon then leaves an imprint on the CMB photons (since it did couple to baryons) and provides us a standard ruler at $z = 1100$! This ruler then can be used in the same way as parallax, i.e., using angular size of sound horizon to determine the angular diameter distance to CMB. Therefore we obtain yet another anchor and due to extremely precise measurements of CMB we can even determine H_0 using CMB alone.

2.2 Tension on H_0 between Supernovae and CMB Measurements

As mentioned in the last section, in addition to the distance ladder in the low redshift, one can also use CMB to determine the value of H_0. However both values depends on the underlying cosmological model. The SNe measurement requires multiple anchors and thus surfers from the possible contamination due to local inhomogeneity. For CMB measurement the determination of the sound horizon is even more model dependent. Nevertheless, one can still compare the two values directly under the same model.

For vanilla FRW model, H_0 is determined as

$$H_0^{SN} = 73.24 \pm 1.74 \, kms^{-1}Mpc^{-1} \, , \tag{2.4}$$

$$H_0^{CMB} = 66.93 \pm 0.62 \, kms^{-1}Mpc^{-1} \, , \tag{2.5}$$

where H_0^{SN} comes from Riess [3], and H_0^{CMB} comes from PLANCK2016 data [4]. A 3.4 σ difference between the two is 99.9% not a fluke, and such strong tension implies that indeed there are contaminations from either the model-choosing process or the systematics of the measurement. Considering the fact that PLANCK, WMAP, and various baryon acoustic oscillation-based results all lead to H_0 around 66 to 69, while according to [3] all anchors leads to H_0 around 72 to 74 (ignoring MW cepheids as they are heavily contaminated by the peculiar motion), it seems highly unlikely that such systematic error would exist. The only possibility remaining is that new physics beyond traditional FRW model must be considered.

We provide an easy way to ease the tension, by considering the possibility that local inhomogeneities may contaminate certain important anchors and ruin the entire cosmic ladder. According to [7], there seems to be a large void nearby, and interestingly the cepheids Riess used to determine the absolute magnitude of SNe are mostly very close to the void, further strengthened the possibility of such contamination. In the next three chapters we will show that indeed the inconsistency between SNe and CMB measurements could be explained by the local inhomogeneities.

doi:10.6342/NTU201603461

國立臺灣大學 · 愛國 · 愛人 · 敬業 · 樂群 ·

doi:10.6342/NTU201603461

Chapter 3

Inhomogeneity of the Universe

Since what we are interested in is the low redshift SNe and cepheids, the cosmological constant is negligible. We will ignore it from now on, except when constructing the density contrast where the background is chosen to be FRW model with PLANCK2016 parameters [4].

Considering the fact that lights also get attracted by the gravitational field, an overdense region would attract more light, thus decreases the observed luminosity distance. In linear limit one would think that an underdense region would be less attractive than nearby region and increases the observed luminosity distance. One can draw the same conclusion from the lensing equation

$$\kappa = \frac{3}{2} H_0^2 \Omega_m \int_0^{\chi_S} d\chi \frac{\chi_S - \chi}{\chi_S} \chi \delta_C(\chi)(1+z)\,, \tag{3.1}$$

where $\kappa = D_0/D_{mod} - 1$ is the convergence of the light, D_{mod} is the altered luminosity distance, Ω_m is the matter density ratio, δ_C is the density contrast, χ is the comoving distance and χ_S is the comoving distance to the source. As we can see

$$\left(\frac{D_{mod}}{D_0}\right)'(z) \propto -\delta_C(z) \tag{3.2}$$

when z is small. Another effect comes from the Doppler effect of the matter outflow due to inhomogeneity. The authors in [8] have calculated the Doppler effect through the velocity field. However these perturbative results actually require δ_C to be small. When this is not the case we must use the full nonlinear EFE. To simplify the calculation, people usually focus on certain types of restricted models.

In the case of a radially inhomogeneous spherically symmetric dust-like system with an observer at the center, the solution of EFE is the Lemaître-Tolman-Bondi (LTB) metric. This is not an open violation of the Copernican principle, since we only consider it as an approximation to the large scale structures by assuming we are at the center of a void and by ignoring all other voids and filaments around us.

The Lemaître-Tolman-Bondi solution can be written as

$$ds^2 = dt^2 - \frac{(R_{,r})^2\, dr^2}{1 + 2\,E} - R^2 d\Omega^2\,, \tag{3.3}$$

where $R = R(t, r)$ is the angular diameter distance, $E = E(r)$ is an arbitrary function of r.

The EFE gives

$$\left(\frac{\dot{R}}{R}\right)^2 = \frac{2E(r)}{R^2} + \frac{2M(r)}{R^3}\,, \tag{3.4}$$

$$\rho(t, r) = \frac{2M_{,r}}{R^2 R_{,r}}\,, \tag{3.5}$$

with $M = M(r)$ being an arbitrary function of r. The solution can be expressed parametrically in terms of a time variable $\eta = \int^t dt'/R(t', r)$ as

$$\tilde{R}(\eta, r) = \frac{M(r)}{-2E(r)}\left[1 - \cos\left(\sqrt{-2E(r)}\eta\right)\right]\,, \tag{3.6}$$

$$t(\eta, r) = \frac{M(r)}{-2E(r)}\left[\eta - \frac{1}{\sqrt{-2E(r)}}\sin\left(\sqrt{-2E(r)}\eta\right)\right] + t_b(r)\,, \tag{3.7}$$

where $\tilde{R}$ has been introduced to clarify the distinction between the two functions $R(t, r)$ and $\tilde{R}(\eta, r)$ which are trivially related by $R(t, r) = \tilde{R}(\eta(t, r), r)$, and $t_b(r)$ is another arbitrary function of r, called the bang function, which corresponds to the fact that big-bang/crunches can happen at different times.

We introduce the variables

$$a(t, r) = \frac{R(t, r)}{r}, \quad k(r) = -\frac{2E(r)}{r^2}, \quad \rho_0(r) = \frac{6M(r)}{r^3}\,, \tag{3.8}$$

so that EFE are written in a form similar to those for the FRW metric:

$$ds^2 = dt^2 - a^2\left[\left(1 + \frac{a_{,r}\, r}{a}\right)^2 \frac{dr^2}{1 - k(r) r^2} + r^2 d\Omega_2^2\right]\,, \tag{3.9}$$

$$\left(\frac{\dot{a}}{a}\right)^2 = -\frac{k(r)}{a^2} + \frac{\rho_0(r)}{3a^3}\,, \tag{3.10}$$

$$\rho(t, r) = \frac{(\rho_0 r^3)_{,r}}{3a^2 r^2 (ar)_{,r}}\,. \tag{3.11}$$

The solution of equations above can now be written using η as

$$\tilde{a}(\tilde{\eta}, r) = \frac{\rho_0(r)}{6k(r)}\left[1 - \cos\left(\sqrt{k(r)}\,\tilde{\eta}\right)\right]\,, \tag{3.12}$$

$$t(\tilde{\eta}, r) = \frac{\rho_0(r)}{6k(r)}\left[\tilde{\eta} - \frac{1}{\sqrt{k(r)}}\sin\left(\sqrt{k(r)}\,\tilde{\eta}\right)\right] + t_b(r)\,, \tag{3.13}$$

where $\tilde{\eta} \equiv \eta \, r = \int^t dt'/a(t', r)\,$.

Clearly we can see that the density $\rho(t, r)$ is directly related to the scale factor a which is then related to spatial curvature $k(r)$. Therefore one can easily describe the inhomogeneity in terms of the luminosity distance which is exactly $(1 + z)^2 R$. This relation involves the inversion of the radial null geodesic equations, and is called the inversion problem, which will be discussed in ch. 5. In the rest of the thesis we will use this last set of equations with simultaneous big bang $t_b = 0$ and drop the tilde to make the notation simpler. Furthermore, without loss of generality, we may set the function $\rho_0(r)$ to be a constant $\rho_0(r) = \rho_0 =$ constant.

doi:10.6342/NTU201603461

Chapter 4

Data Analysis

Our targets of interest are the low redshift SNe and cepheids that affect H_0 measurement considerably. To do so we need a clean dataset. Our dataset comes from two different groups. For SNe the data comes from Union2.1 catalogue [5], and for the cepheids the data comes from Riess' 2016 paper [3]. We calibrate the old Union2.1 data according to the difference between Riess' new result and the old calibrator Union 2.1 catalogue was using [6], by the formula

$$\begin{aligned} m - M &= 25 - 5\log_{10} H_0 + 5\log_{10}(H_0 d_L) \\ &\approx 25 - 5\log_{10} H_0 + 5\log_{10} z\,. \end{aligned} \tag{4.1}$$

To investigate the effect of the inhomogeneity we further include the angular position data from SIMBAD astronomical database. This complete database thus allows us to construct a fit that takes directional dependence into account. We construct a fitting program that helps us extracting a model-independent global fitting formula for the luminosity distance, as will be discussed in the following sections.

4.1 Linear Regression and χ^2 Analysis

Given a dataset with N data points one of the simplest way to obtain a smooth function is the linear regression

$$f(\vec{X}) = \sum_{m=1}^{n} w_m b_m(\vec{X})\,, \tag{4.2}$$

where b_m is the m-th basis and w_m is the associated weight. The total number of basis n is restricted to be no greater than the number of data points, such that the system is not under-determined. To obtain the best fit weight one tries to minimize the total error of the

doi:10.6342/NTU201603461

fit in terms of χ^2:

$$\chi^2 = \sum_{i=1}^{N} \left(\frac{y_i - f_i}{e_i} \right)^2 , \tag{4.3}$$

where y_i is the i-th data point value, e_i is the associated error, and f_i is the fitted value $f(\vec{X}_i)$ at i-th data point position $\vec{X}_i$. Assuming Gaussian distribution of error the likelihood of fitted values $\{f_i\}$ would be $e^{-\chi^2}$, and the minimization process is equivalent to the maximization of the likelihood of the fit. Such best fit can be described as

$$\mathbf{W} = \mathbf{H}^{-1} \cdot \mathbf{Y}_W , \tag{4.4}$$

where $\mathbf{Y}_W \equiv \{y_i/e_i\}$, $\mathbf{W} \equiv \{w_m\}$, $\mathbf{H} = h_{im} = e_i^{-1} b_m(\vec{X}_i)$, and the inverse here is the Moore-Penrose pseudo-inverse that minimizes χ^2.

To visualize this process one can imagine that the fitting likelihood distribution is a n-dimensional Gaussian distribution in the $\mathbb{R}^n$ space of $\{(y_i - f_i)/e_i\}$, and a null fit $f = 0$ is at $\mathbf{Y}_W$ position. A linear regression fit can be visualized as the closest point to the origin on a hyperplane of dimension n spanned by $\mathbf{H}$ passing through $\mathbf{Y}_W$. We can therefore separate χ^2 into an unexplained part (distance from the origin to that closest point) and an explained part (distance from the closest point to the null fit point). We may also calculate the probability distribution of χ^2 on a n-d plane with residual $\chi^2 = \chi_0^2$ as

$$P(\chi^2) = \pi^{-n/2} \int_0^{\chi - \chi_0} e^{-x^2} V(\mathbb{S}^{n-1}) dx^n , \tag{4.5}$$

where $V(\mathbb{S}^{n-1})$ is the volume of a standard $(n-1)$ dimensional ball. This is the famous cumulative probability of the χ^2 distribution. The so called 68% or 95% confidence band is precisely the envelop of all possible fits that have accumulative probability less than 68% or 95%. At first sight the computation of the envelop seems to be an extremely complicated process, but luckily for linear regression the boundary of the envelop is the same as a hypersphere on the hyperplane with radius given by the inversion of $P(\chi^2)$. Such hypersphere can be directly written down as

$$\frac{\chi_P^2 - \chi_0^2}{n} = tr \left(\mathbf{H} \cdot \delta \mathbf{W} \right)^2 = \frac{\chi_P^2 - \chi_0^2}{n} tr \left(\mathbf{H} \cdot \mathbf{H}^{-1} \cdot \mathbf{n} \right)^2 , \tag{4.6}$$

where $\delta\mathbf{W}$ is the change of the weight on the boundry, and $\mathbf{n}$ is an arbitrary unit vector. By Cauchy inequality the boundary of the envelop can be described as

$$\pm \sup\{\mathbf{B} \cdot \delta\mathbf{W}\} \propto \pm \sup_{\mathbf{n}} \{\mathbf{B} \cdot \mathbf{H}^{-1} \cdot \mathbf{n}\} = \pm \left| \mathbf{B} \cdot \mathbf{H}^{-1} \right| , \tag{4.7}$$

where $\mathbf{B} = \{b_m\}$ is the n-dimensional basis vector.

4.2 Monte Carlo + Local Optimization

A natural extension to the linear regression model would be the inclusion of non-linear parameters

$$f(\vec{X}) = \sum_{m=1}^{n} w_m b_m(\{p_{am}\}\,;\,\vec{X})\,, \tag{4.8}$$

where $\{p_{am}\}$ are some nonlinear parameters for basis b_m. Assuming there are k non-linear parameters in total, one can again visualize the fitting process as finding the minimum on a $n + k$ dimensional curved hypersurface. Since it is no longer a linear/flat system, many linear algebra techniques we used in the last section do not apply. The only two methods remaining are Monte Carlo method and local optimization method.

Local optimization method, as its name suggests, is the usual variational method when searching for a local minimum. Since usually the basis is analytic, one can easily compute the gradient of χ^2 and use the steepest descend method to approach the local minimum in an iterative way. But just like the search of the ground state in a many-body QM system, most of the time a local minimum is not the global minimum. Therefore we need a complementary method that allows us to probe lots of local minima and then pick the minimum of local minima as the probed global minimum. Randomly generating a list of initial points on the hypersurface, i.e., the Monte Carlo (MC) method, fits our need perfectly. One of the most annoying problem of MC method is that one needs a prior probability distribution of parameters to generate a list of initial points that are "reasonably good". Luckily for us the basis we chose has a very special form:

$$b_m(\vec{X}) = \Phi\left(\left|\vec{X} - \vec{X}_m\right|\right)\,, \tag{4.9}$$

where Φ is a very simple monotonic function ($r^{2L}\ln r$ or r^{2L+1} for $L \in \mathbb{N}$), and $\vec{X}_m$ are the non-linear parameters. Using monotonic function as the basis requires them to be put as close to the data points as possible, so one gets a reasonable prior distribution from the distribution of the data points. To speed up the MC process further, we optimize the distribution by rebuilding the distribution using the parameters emitted by the local optimization program. By doing so we speed up the MC process by more than 100 times.

Once we get the best fit from MC plus local optimization, we can regard its fitting χ^2 as the unexplained part of the χ^2 distribution and find the corresponding χ^2 for the P-confidence band. Here we make an approximation that the hypersurface is almost flat, since it is computationally forbidden to construct the hypersurface integral. The error of χ^2 introduced through this way is of the order $\bar{R}$, the average of the scalar curvature on the hypersurface around the best fit. Usually $\bar{R}$ is small, and the approximation is valid. The envelop of all possible fits that have χ^2 smaller than what is obtained for the P-confidence

doi:10.6342/NTU201603461

band, would be the P-confidence band for the nonlinear fit. For outliers we follow the routine in Riess' 2016 paper [3], i.e. the classic "global but removing single largest outlier at a time" method. For a complete work-flow chart please see fig. 4.1.

doi:10.6342/NTU201603461

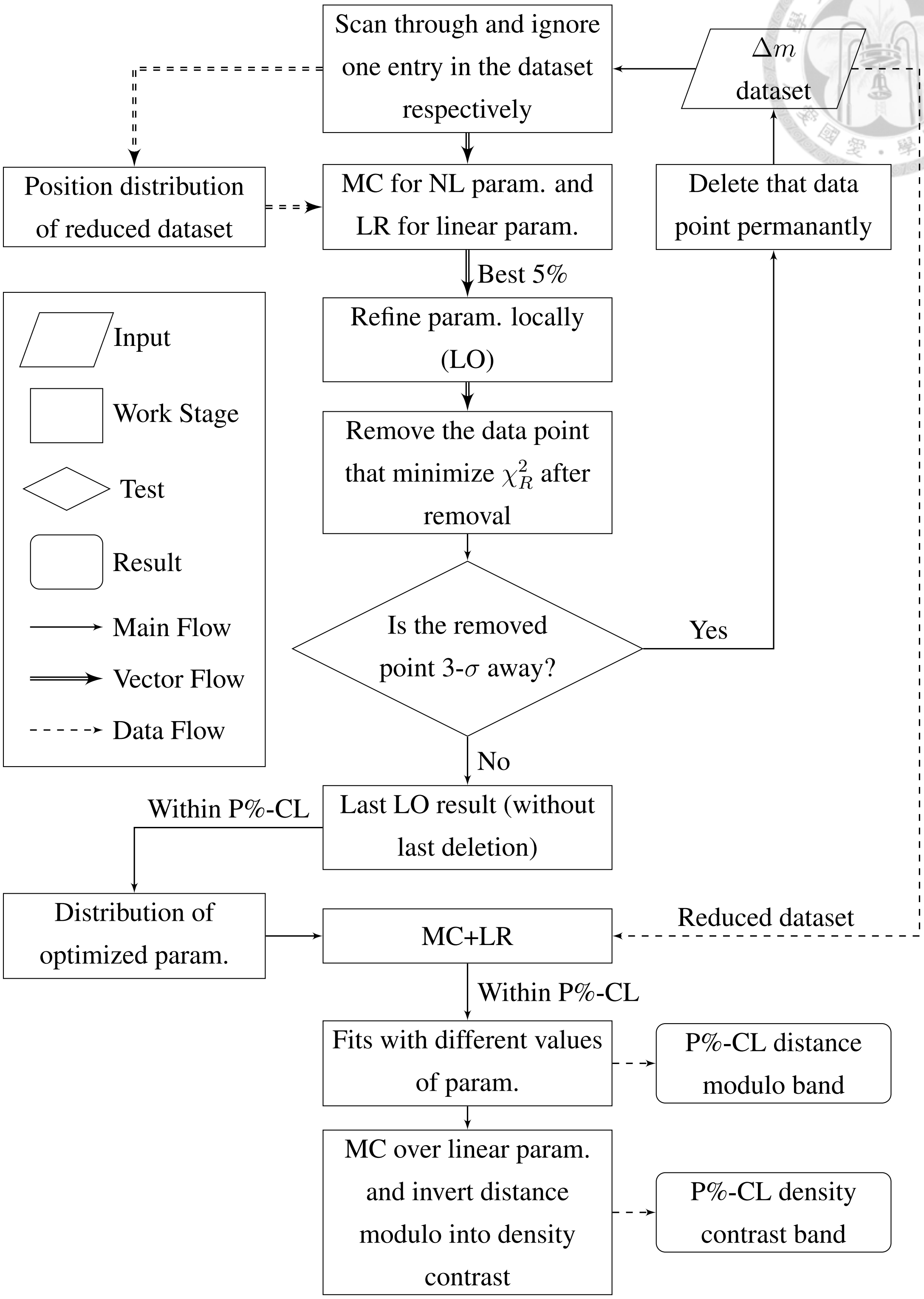
Scan through and ignore one entry in the dataset respectively
Δm dataset
Position distribution of reduced dataset
MC for NL param. and LR for linear param.
Delete that data point permanantly
Best 5%
Refine param. locally (LO)
Input
Work Stage
Test
Result
Main Flow
Vector Flow
Data Flow
Remove the data point that minimize χ^2_R after removal
Is the removed point 3-σ away?
Yes
No
Within P%-CL
Last LO result (without last deletion)
Distribution of optimized param.
MC+LR
Reduced dataset
Within P%-CL
Fits with different values of param.
P%-CL distance modulo band
MC over linear param. and invert distance modulo into density contrast
P%-CL density contrast band

Figure 4.1: Work-flow of the fitting procedure. Δm stands for difference between observed magnitude and the predicted value from the FRW model with PLANCK 2016 parameters. Here LR stands for lineara regression, NL for nonlinear, param. for parameters, and CL for confidence level. The double arrow consists of n copies of flows, each of which has a different data point deleted. The idea of inversion will be introduced in the next chapter.

doi:10.6342/NTU201603461

doi:10.6342/NTU201603461

Chapter 5

Easing H_0 Tension by Invoking Local Inhomogeneity

In this chapter we will talk about the inversion method and show the comparison between density contrast derived from the inversion method using observed luminosity distance fitted previously and the observed density contrast from the galaxy survey.

5.1 Geodesic Equation and the Initial Condition

The luminosity distance for an observer at the center of a LTB space as a function of the redshift is given by

$$D_L(z) = (1+z)^2 R\left(t(z), r(z)\right) = (1+z)^2 r(z) a\left(\eta(z), r(z)\right) \,, \tag{5.1}$$

where $\Big(t(z), r(z)\Big)$ or $\Big((\eta(z), r(z)\Big)$ is the solution of the radial null geodesic equations. The past-directed radial null geodesic is given by

$$\frac{dT(r)}{dr} = f(T(r), r)\,, \quad f(t,r) = \frac{-R_{,r}(t,r)}{\sqrt{1+2E(r)}}\,, \tag{5.2}$$

where $T(r)$ is the time coordinate along the geodesic as a function of the coordinate r. Applying the definition of redshift it is possible to obtain

$$\frac{d\eta}{dz} = \frac{\partial_r t(\eta, r) - F(\eta, r)}{(1+z)\partial_\eta F(\eta, r)} = p(\eta, r)\,, \tag{5.3}$$

$$\frac{dr}{dz} = -\frac{a(\eta, r)}{(1+z)\partial_\eta F(\eta, r)} = q(\eta, r)\,. \tag{5.4}$$

where we have used the following identities

$$\begin{aligned}
f(t(\eta,r),r) &= F(\eta,r)\,, \qquad (5.5)\\
\dot{f}(t(\eta,r),r) &= \frac{1}{a}\partial_\eta F(\eta,r)\,, \qquad (5.6)\\
R_{,r}(t,r) &= \partial_r R(t(\eta,r),r) + \partial_\eta R(t(\eta,r),r)\partial_r\eta\,, \qquad (5.7)\\
F(\eta,r) &= -\frac{1}{\sqrt{1-k(r)r^2}}\left[\partial_r(a(\eta,r)r) + \partial_\eta(a(\eta,r)r)\partial_r\eta\right]\\
&= -\frac{1}{\sqrt{1-k(r)r^2}}\left[\partial_r(a(\eta,r)r) - \partial_\eta(a(\eta,r)r)a(\eta,r)^{-1}\partial_r t\right]\,. \qquad (5.8)
\end{aligned}$$

The functions p, q, F have an explicit analytical form which can be obtained from $a(\eta,r)$ and $t(\eta,r)$. Using this approach the coefficients of geodesic equations are fully analytical, which is a significant improvement over previous methods which required a numerical integration of the Einstein's equations to obtain the function $R(t,r)$.

Before deriving the set of differential equations for the solution of the inversion method it is important to analyze how many independent initial conditions we need to fix. Our final goal will be to set and solve a set of differential equations in redshift space starting from the center, where by definition $z = 0$. Given our choice of coordinates the model will be fully determined by the functions $k(z), r(z), \eta(z)$, corresponding to three initial conditions

$$\begin{aligned}
r(0) &= 0\\
\eta(0) &= \eta_0\\
k(0) &= k_0\,. \qquad (5.9)
\end{aligned}$$

The system of differential equation we will derive only involves derivatives of order one respect to the redshift, so these initial conditions will be enough. Given the assumption of the central location of the observer we have $r_0 = 0$, while the observed value of the local Hubble parameter H_0 corresponds to another constraint among the central values k_0, η_0, so only one of them is independent. After defining the Hubble rate as

$$H^{LTB} = \frac{\partial_t a(t,r)}{a(t,r)} = \frac{\partial_\eta a(\eta,r)}{a(\eta,r)^2} \qquad (5.10)$$

we need to impose the two following conditions

$$\begin{aligned}
a(\eta_0,0) &= a_0\,, \qquad (5.11)\\
H^{LTB}(\eta_0,0) &= H_0, \qquad (5.12)
\end{aligned}$$

where a_0 is, as expected, an arbitrary parameter, η_0 is the value of the generalized conformal time coordinate η corresponding to the central observer today, and H_0 is the observed value of the local Hubble parameter.

After re-writing the solution in terms of the following more convenient dimensionless quantities

$$a(T,r) = \frac{a_0 \Omega_M^0 \sin^2\left(\frac{1}{2} T \sqrt{K(r)}\right)}{K(r)}\,, \tag{5.13}$$

$$t(T,r) = H_0^{-1} \frac{\Omega_M^0}{2K(r)} \left[T - \frac{1}{\sqrt{K(r)}} \sin\left(\sqrt{K(r)}\,T\right)\right] + t_b(r)\,, \tag{5.14}$$

$$k(r) = (a_0 H_0)^2 K(r)\,, \tag{5.15}$$

$$\eta = T (a_0 H_0)^{-1}\,, \tag{5.16}$$

$$\rho_0 = 3 \Omega_m^0 a_0^3 H_0^2\,. \tag{5.17}$$

We can impose two conditions $a(\eta_0, 0) = a_0$ and $H^{LTB}(\eta_0, 0) = H_0$ for Ω_M^0 and T_0 to finally get the initial conditions and the exact solution in this form

$$a(T,r) = \frac{a_0 (K_0 + 1) \sin^2\left(\frac{1}{2} T \sqrt{K(r)}\right)}{K(r)}\,, \tag{5.18}$$

$$t(T,r) = H_0^{-1} \frac{1 + K_0}{2K(r)} \left[T - \frac{1}{\sqrt{K(r)}} \sin\left(\sqrt{K(r)}\,T\right)\right] + t_b(r)\,, \tag{5.19}$$

$$K_0 = K(0)\,, \tag{5.20}$$

$$T_0 = \frac{\arctan\left(2\sqrt{K_0}\right)}{\sqrt{K_0}}\,, \tag{5.21}$$

$$\Omega_m^0 = K_0 + 1\,. \tag{5.22}$$

Since we have three unknown $\{\Omega_m^0, T_0, K_0\}$ and two constraints, one of them can always remain free, and the other two can be expressed in terms of it. Here we chose K_0 to be the free parameter, but we could equivalently chose another one. The above form of the solution is particularly useful to explore the full class of LTB models. Since K_0 is a free parameter which determines the central value of the dimensionless conformal time variable T_0, the realness condition sets a lower bound $K_0 > -1$. H_0 is also a free parameter which can be set according to observations and fixes the scale for the definition of the dimensionless quantities $K(r), T, \Omega_m^0$. This means that we can arbitrarily fix K_0 and H_0 as long as we impose the correct initial condition given above.

As expected a_0 does not appear in observable quantities such as the cosmic time $t(\eta, r)$, and it can be fixed to 1. In this way we can self-consistently determine all the necessary initial conditions and we are left with the freedom to fix K_0 arbitrarily. As we will see later actually the change of K_0 does not modify the density contrast too much, so the model is determined once D_L is given.

5.2 Mapping D_L back to Density Contrast

In the previous section we have seen that it is possible to derive a fully analytical set of radial null geodesics equations. Our goal now is to use these equations to obtain a new set of differential equations to map an observed $D_L(z)$ to a LTB model. In the coordinates we chose, a LTB solution is determined uniquely by the function $k(r)$, so we will have a total of three independent functions to solve for $\eta(z), r(z), k(z)$. Since we have already two differential equation for the geodesics, we need an extra differential equation.

This can be obtained by differentiating with respect to the redshift the luminosity distance $D_L(z)$

$$\frac{d}{dz}\left(\frac{D_L^{obs}(z)}{(1+z)^2}\right) = \frac{\partial(ra(\eta,r))}{\partial\eta}\frac{d\eta}{dz} + \frac{\partial(ra(\eta,r))}{\partial r}\frac{dr}{dz} = s(z) \tag{5.23}$$

where $D_L^{obs}(z)$ is the observed luminosity distance. In our case we will use the best fit function obtained using the method developed in ch.4. Now we have the set of equations we were looking for

$$\frac{d\eta}{dz} = p(\eta(z), r(z)) = p(z)\,, \tag{5.24}$$
$$\frac{dr}{dz} = q(\eta(z), r(z)) = q(z)\,, \tag{5.25}$$
$$\frac{d}{dz}\left(\frac{D_L^{obs}(z)}{(1+z)^2}\right) = s(z)\,. \tag{5.26}$$

Since we will solve our differential equations with respect to the the variable z, we need to transform the partial derivatives respect to η and r in eqs.(5.3,5.4) according to the chain rule:

$$\left.\frac{\partial h(\eta,r)}{\partial r}\right|_{(\eta=\eta(z),r=r(z))} = \frac{\partial h(\eta(z),r(z))}{dz}\frac{dz}{dr}\,, \tag{5.27}$$
$$\left.\frac{\partial h(\eta,r)}{\partial\eta}\right|_{(\eta=\eta(z),r=r(z))} = \frac{\partial h(\eta(z),r(z))}{dz}\frac{dz}{d\eta}\,. \tag{5.28}$$

where $h(\eta, r)$ is a generic function in the coordinates (η, r). After this substitution the equations contain only functions of the redshift z, and derivatives respect to z. The differential equations obtained in this form need to be further manipulated in order to re-write them in a canonical form in which the derivatives appear all on one side, since after the application of the chain rule to eqs.(5.3,5.4) derivative terms like $\frac{dr(z)}{dz}$, $\frac{d\eta(z)}{dz}$, $\frac{dk(z)}{dz}$ are also on the right-hand side. After a rather complicated algebraic manipulation done using

doi:10.6342/NTU201603461

MATHEMATICA™ we get :

$$\begin{aligned}
0 &= 4t^2K'(z)\Big((3+2t^2)\sqrt{K(z)}r(z)+(3+t^2)SX-3tS\Big)-8t^3(1+z)K(z)^2r'(z)T'(z)\\
&\quad-2tK(z)r(z)K'(z)(3(1+t^2)T(z)+(3+5t^2)(1+z)T'(z))\\
&\quad+K(z)^{3/2}(-8t^4r'(z)+3(1+t^2)^2(1+z)r(z)T(z)K'(z)T'(z))
\end{aligned}\tag{5.29}$$

$$\begin{aligned}
0 &= 2t(1+z)\left((3+5t^2)r(z)K'(z)+4t^2K(z)r'(z)\right)\\
&\quad-8\sqrt{K(z)}t^4S+6(1+t^2)^2(1+z)r(z)XK(z)
\end{aligned}\tag{5.30}$$

$$\begin{aligned}
0 &= 2K(z)\left((1+K_0)t^2r'(z)-(1+t^2)K(z)H_0\frac{d}{dz}\left(\frac{D_L^{obs}(z)}{(1+z)^2}\right)\right)\\
&\quad-2(1+K_0)t\,r(z)\left((t-X)\,K(z)-K(z)^{3/2}T'(z)\right)
\end{aligned}\tag{5.31}$$

In the above expressions we have expressed all the trigonometric functions in terms of the equivalent expressions in terms of $\tan(X)$ according to

$$S=\sqrt{1-K(z)r(z)^2}\,,\tag{5.32}$$

$$t=\tan(X)\,,\tag{5.33}$$

$$X=\frac{1}{2}\sqrt{K(z)}T(z)\,.\tag{5.34}$$

We have also used the dimensionless version of the solution in terms of $K(z), T(z)$ derived in the previous section.

As it can be seen the above three equations are not linear in the derivative terms, but the second one only involves $\{r'(z), K'(z)\}$, while the other two involve all the three functions $\{r'(z), K'(z), T'(z)\}$. This suggests that we can first solve for $r'(z)$ in terms of only $K'(z)$:

$$\begin{aligned}
r'(z) &= \frac{1}{8t^3(1+z)K(z)}\Bigg[8t^4\sqrt{K(z)}S-6(1+z)t\,r(z)K'(z)\\
&\qquad-10(1+z)t^3r(z)K'(z)+6Xr(z)K'(z)(1+z)\left(1+t^2\right)^2\Bigg]
\end{aligned}\tag{5.35}$$

and then substitute into other 2 eqs. to get:

$$\begin{aligned}
K'(z) &= t(2tK(z)^{3/2}\left(9(1+t^2)r(z)+(3+t^2)ST(z)\right)\\
&\quad-4t^2SK(z)\left(3-2t\sqrt{K(z)}T'(z)\right)\\
&\quad-K(z)(8t^4S\,(1+z)^{-1}+3(3+4t^2+t^4)r(z)T(z)K(z)))
\end{aligned}\tag{5.36}$$

$$\begin{aligned}
T'(z) &= \frac{1+K_0}{4t}(-6t(1+3t^2)r(z)K(z)+\sqrt{K(z)}(8t^4S\,(1+z)^{-1}\\
&\quad+(3+10t^2+3t^4)r(z)T(z)K(z))+8t^2K(z)^{3/2}r(z)T'(z)\\
&\quad-8t(1+t^2)\,(1+K_0)^{-1}\,K(z)^2H_0\frac{d}{dz}\left(\frac{D_L^{obs}(z)}{(1+z)^2}\right))
\end{aligned}\tag{5.37}$$

These two equations now only involve $K'(z), T'(z)$ in a linear form, so they can be solved directly, and then the result for $K'(z)$ can be substituted in the equation for $r'(z)$. After some rather cumbersome algebraic manipulations we finally get:

$$\begin{aligned}
\frac{dT(z)}{dz} =& \frac{2\sqrt{K(z)}}{3t(1+K_0)r(z)} \times \left[Rz(z) \left(1 + \frac{(1+3t^2)\sqrt{K(z)}r(z)}{2\left(\sqrt{K(z)}r(z) - t\,S\right)} \right) \right. \\
& \left. - \frac{(1+K_0)t^3 S}{(1+t^2)(1+z)K(z)^{3/2}} \right], \qquad (5.38) \\
\frac{dr(z)}{dz} =& -\frac{S}{3\,t\,(t^2X - 3t + 3X)} \times \left[\frac{Rz(z)K(z)\left(t\,(3+5t^2) - 3\,(1+t^2)^2\,X\right)}{(1+K_0)\left(-\sqrt{K(z)}r(z) + t\,S\right)} \right. \\
& \left. + \frac{2\,t^2\,(2t^3 - 3t^2X + 3t - 3X)}{(1+t^2)\,(1+z)\sqrt{K(z)}} \right], \qquad (5.39) \\
\frac{dK(z)}{dz} =& \frac{4t^2\sqrt{K(z)}Rz(z)}{3(1+K_0)\,(1+t^2)\,(1+z)r(z)\,(t^2X - 3t + 3X)} \times \\
& \left[\frac{Rz(z)\,(1+t^2)\,(1+z)K(z)^{3/2}}{-\sqrt{K(z)}r(z) + t\,S} - (1+K_0)t^2 \right], \qquad (5.40)
\end{aligned}$$

where $Rz(z) = H_0 \frac{d}{dz}\left(\frac{D_L^{obs}(z)}{(1+z)^2}\right)$.

The density can be expressed as

$$\begin{aligned}
\rho =& \frac{H_0\,(1+t^2)^2\,k(z)^3}{(1+K_0)t^4} \left(\frac{H_0\left(3\,(1+t^2)^2\,X - 3t - 5t^3\right)}{(1+K_0)t^2\,(t^2X - 3t + 3X)} \right. \\
& \left. + \frac{2\left(\sqrt{1-S^2} - St\right)(2t^3 - 3t^2X + 3t - 3X)}{(1+z)Rz(z)\,(1+t^2)\,k(z)^{3/2}\,(t^2X - 3t + 3X)} \right). \qquad (5.41)
\end{aligned}$$

Now we are ready to convert the luminosity distance into the density contrast.

5.3 Result

Here we show our preliminary results. Since we have not yet obtained the data from Keenan [7], we are not able to include their plots of observational data of density contrast.

As our goal is to compare our inverted density contrast with the one obtained in [7], we will follow their syntax and define fields 1, 2, 3 as what are shown in fig. 5.1. In the same figure we can also find that only field 1s and 3 contain enough data points, so we will analyze these two fields only. After removing 5 outliers, we successfully fit $m_{obs} - m_{FRW}$ in field 3 with a reduced $\chi^2 \sim 0.77$, and show that indeed SNe in field 3 are brighter than expected in fig.5.2. Statistically the fitting also passes the null hypothesis as the reference

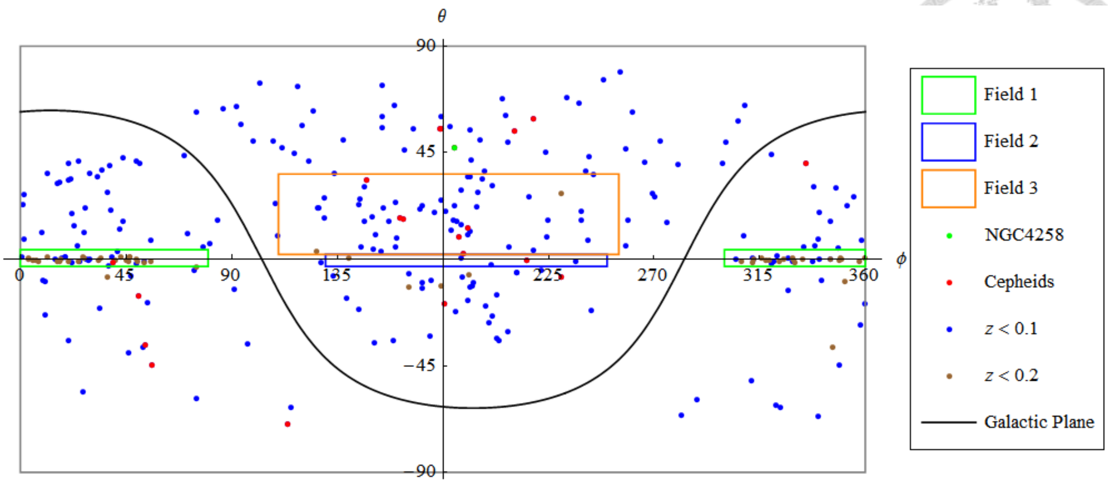

Figure 5.1: This plot shows the sky map of all SNe and cepheids in our dataset. Three fields are specified in Keenan's work [7] as the three regions with density contrast data. Our targets of interest are field 1 and field 3 which contain enough data points to fit the luminosity distance curve. For the sake of clarity we will keep using the same color for field 1 and field 3 as [7] later on.

model [3] has a larger reduced $\chi^2 \sim 0.91$. In contrast as shown in fig.5.3, for field 1 where most higher redshift SNe lie in, the fit we get after removing 4 outliers is a simple shift in magnitude. The reduced $\chi^2 \sim 0.55$ is again much lower than what vanilla FRW model could achieve [3]. Finally we invert each fitted curve within the 68% confidence band and get an envelop for the density contrast as shown in fig.5.4 and 5.5. According to sec.5.1 K_0 is not fixed, but actually the density contrast is almost independent of K_0 as shown in fig.5.6. So we decide to choose a specific $K_0 = -0.1$ as an example since we believe that we are actually in a void. Finally we compare this inverted density profile to the one from [7]. Qualitatively our results for fields 1 and 3 is consistent with what was observed through luminous density, indicating that indeed local structures could alter the luminosity distance significantly.

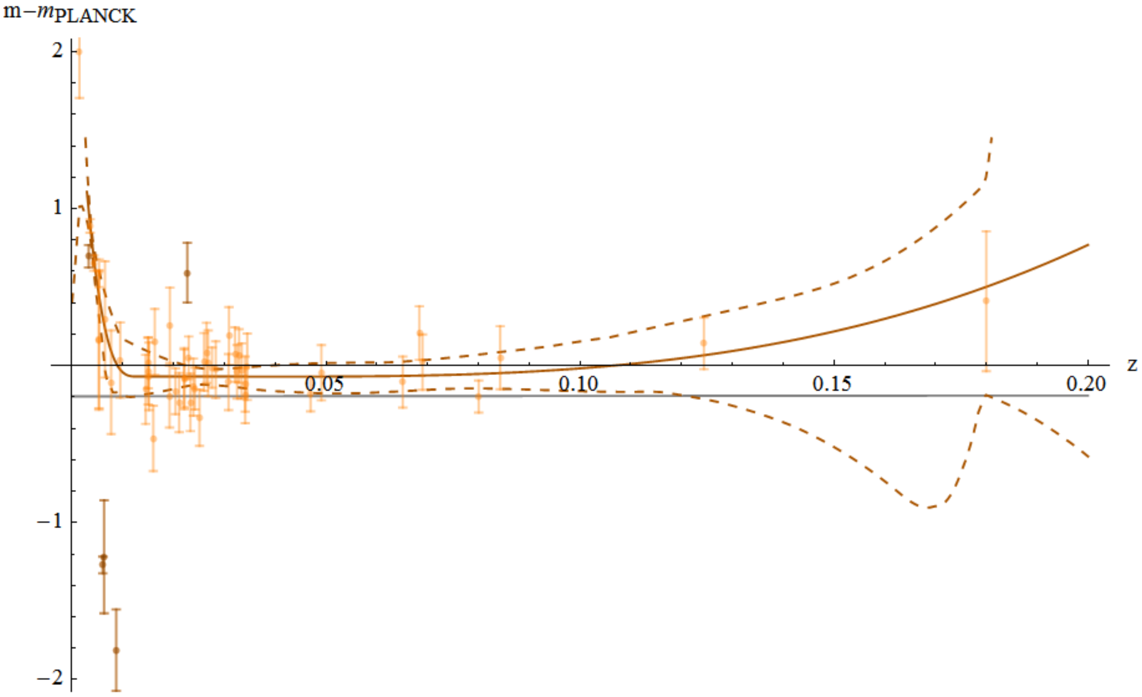

Figure 5.2: This plot shows the 68% confidence band of the field 3 Δm fit, along with the data points in this region. The deleted data points are in a darker color. The dashed curves are the 68% confidence band envelop and the vanilla curve is the best fit. The fitting model is chosen to be 5 functions of the form $\Phi(r) = r^3$ according to the dimensional argument of the polyharmonic spline interpolation method. The gray curve is the result from Riess 2016 [3].

doi:10.6342/NTU201603461

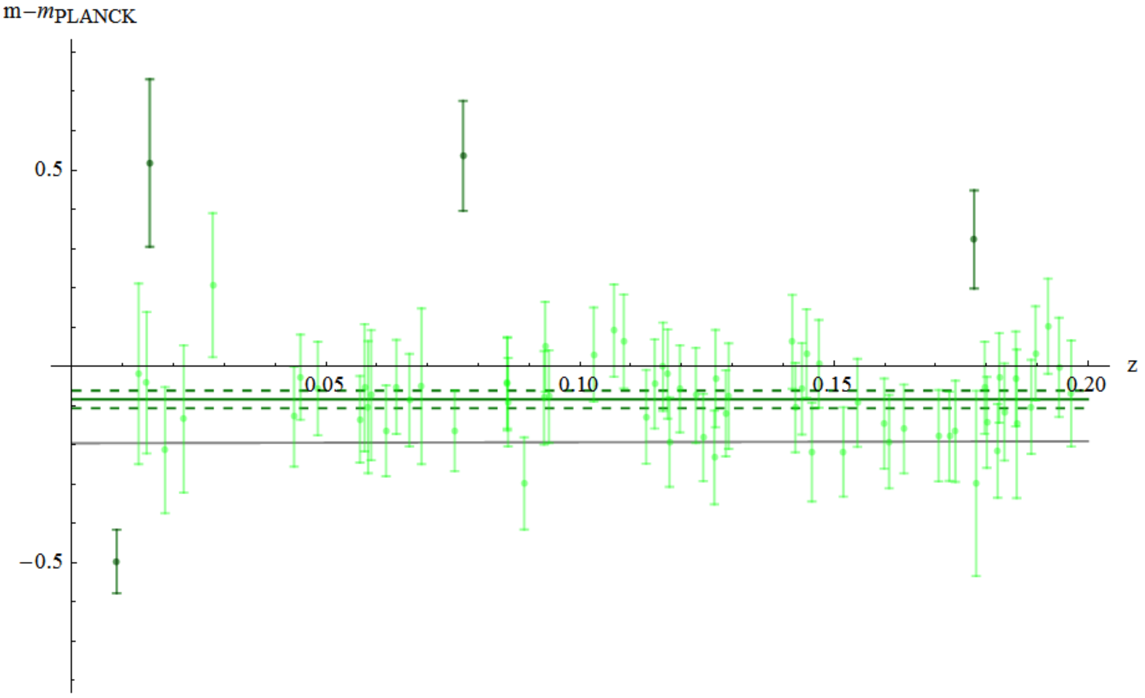

Figure 5.3: This plot shows the 68% confidence band of the field 1 Δm fit, along with the data points in this region. The deleted data points are in a darker color. The dashed curves are the 68% confidence band envelop and the vanilla curve is the best fit. The fitting model is chosen to be a simple constant shift. The gray curve is the result from Riess 2016 [3].

doi:10.6342/NTU201603461

國立臺灣大學 敦品勵學·愛國愛人

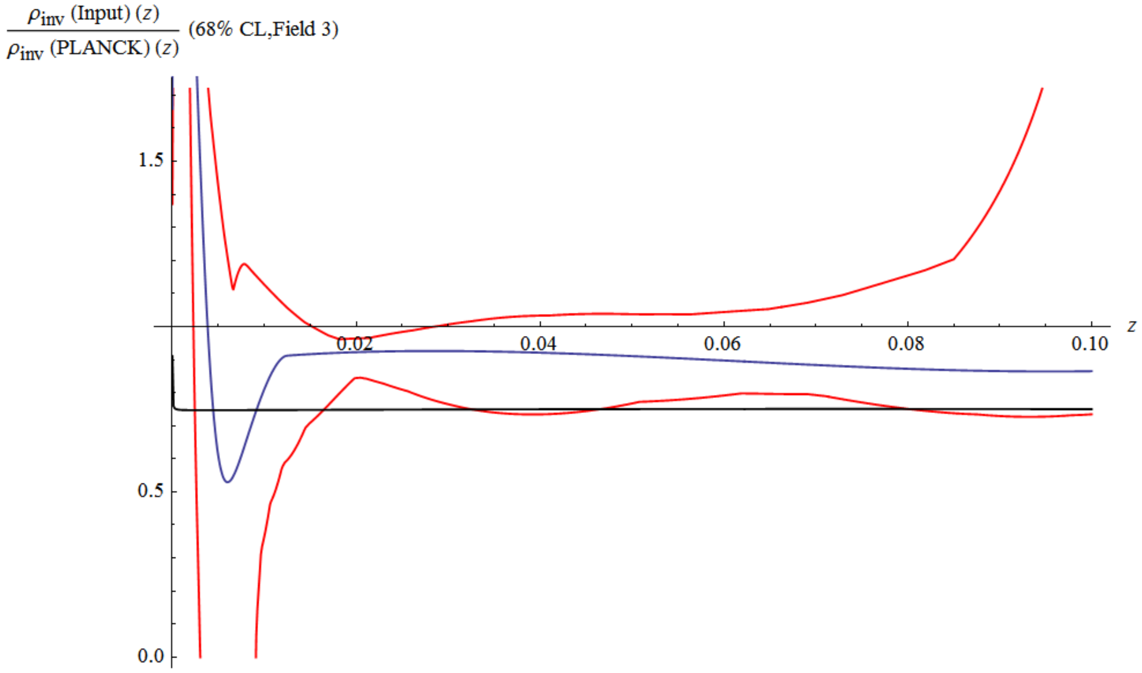

Figure 5.4: This plot shows the 68% confidence band of the inverted density contrast of the field 3, with $K_0 = -0.1$. Clearly we can see a ∼68% significant 10% under-dense around $z = 0.02$ to 0.08 or $100 \sim 400$ Mpc. One can directly compare this plot to Keenan's using conversion $d(Mpc) = H_0^{-1} z = 4400\, z\, Mpc$. One important feature in Keenan's result is the overdense region at around $z = 0.1$, and as we can see such feature is in the 68% confidence band of our result. The gray curve is the inverted density contrast of the FRW model with parameters from Riess 2016 [3].

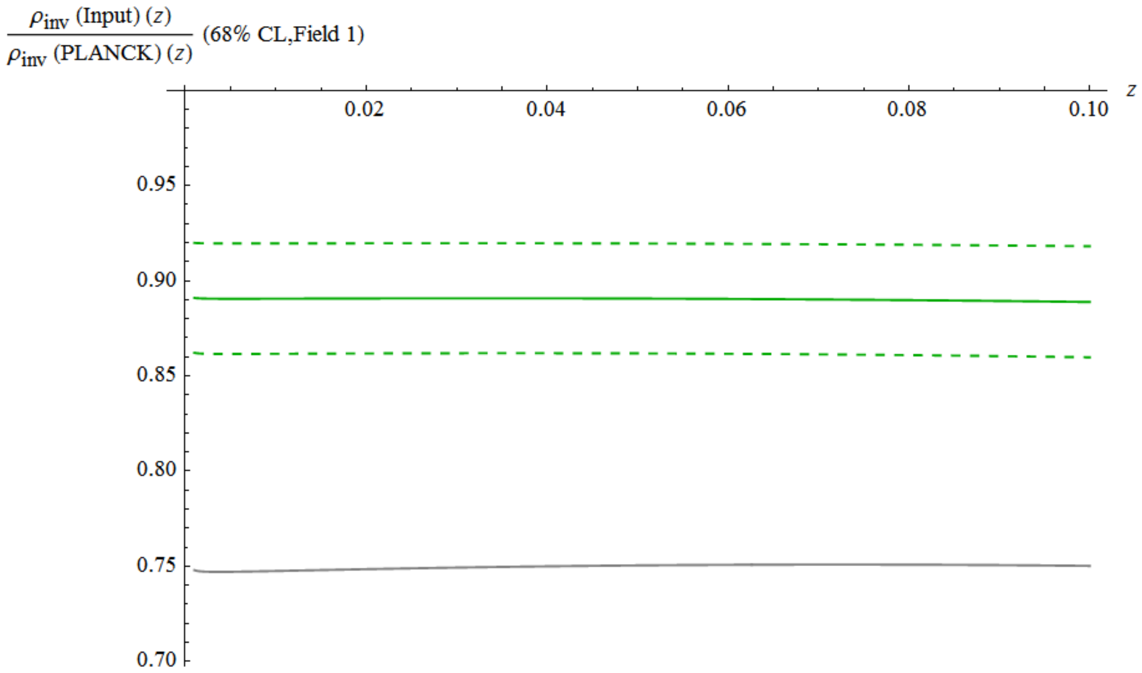

Figure 5.5: This plot shows the 68% confidence band of the inverted density contrast of the field 1, with $K_0 = -0.1$. Clearly we can see a ~95% significant 10% under-dense everywhere. One can directly compare this plot to Keenan's using conversion $d(Mpc) = H_0^{-1} z = 4400\, z\, Mpc$, and find that the two agree with each other pretty well. The gray curve is the inverted density contrast of the FRW model with parameters from Riess 2016 [3].

doi:10.6342/NTU201603461

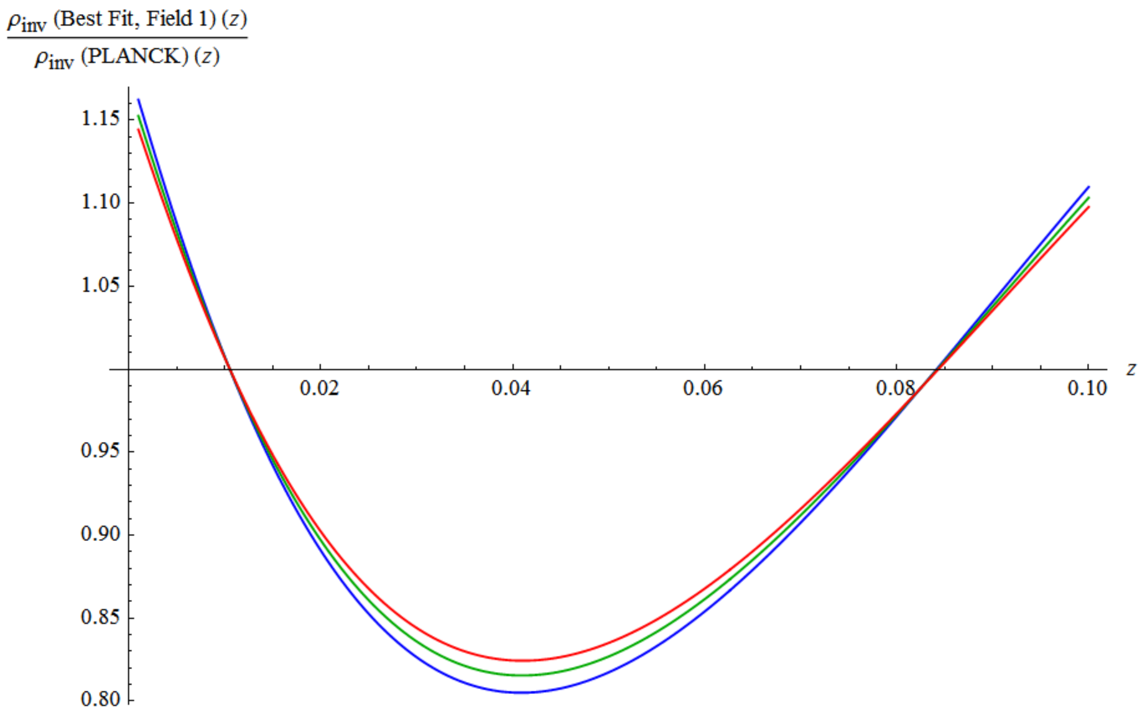

Figure 5.6: This plot shows the inverted density contrast of the best fit in the field 3, under different K_0. The blue, green, red curves correspond to $K_0 = -0.1$, 0, and 0.1 respectively.

doi:10.6342/NTU201603461

Chapter 6

Quantization of Spacetime

In Riemannian geometry, the quadratic distance function g living on a manifold M describes the structure of the tangent bundle TM uniquely through specifying the relation between quadratic line element ds_R^2 and the coordinate difference dx. The quadratic nature of $ds_R^2 = g_{\mu\nu}dx^\mu dx^\nu$ which implies Lorentz symmetry and Pythagorean theorem, is based on numerous experimental facts [10]. It is one of the foundations of GR and even when quantizing gravity, people usually promote it to its quantum version without modification. But in both LQG and superstring theories, the existence of a minimal distance measure suggests that the infinitely-differentiable geometry may be an illusion that ceases to be valid at the smallest scale. This interesting consequence of combining GR with QFT leads to the notion that spacetime structure itself may have to be modified. H.S. Snyder coined this attempt in the name of "quantized space-time" in his seminal article published in 1947 [11].

Currently there are two major routes to tackle the quantization of spacetime. Dimensional reduction from a higher dimensional momentum space proposed by Snyder is a popular approach, which was followed by S. Majid, G. Amelino-Camelia, and others in the construction of their own versions of quantized spacetime [12, 15, 13]. The other route, first introduced by A. Connes [16, 17], comes from partial differential equation analysis on non-commutative space (C^* algebra), where fields and Fourier analysis can be defined classically, with twisted measure providing non-commutativity. This approach has been proven to be extremely versatile in the pursuit of quantized spacetime as non-commutativity usually plays an important role [18, 19, 20, 21].

Here we consider a new way of deforming spacetime algebra, first proposed by R. Adler [22], which has its root in Clifford algebra of the tangent bundle. Instead of a bosonic structure where generators of momentum space serve as the coordinate measures, this theory treats the proper distance measure as the composition of infinite generators of Clifford structure on the tangent bundle of the position space. A continuous geodesic

doi:10.6342/NTU201603461

therefore becomes piecewise-linear and so is the manifold. As we will show by carefully defining the measure, a QM system can be constructed on top of it.

6.1 Dimensional Reduction of Momentum Space

Snyder suggested [11] a deformation stemmed from the exponential map of a 4-d de Sitter (dS) space with "radius" a^{-1} embedded inside a 5-d momentum space ($dk^2_{\mathbb{R}^{1,4}} = dk_0^2 - dk_1^2 - dk_2^2 - dk_3^2 - dk_4^2$), i.e.,

$$a^{-2} = k_0^2 - k_1^2 - k_2^2 - k_3^2 - k_4^2 \,. \tag{6.1}$$

Next, $\hat{x}^\mu$ is chosen to be the momentum translation Killing vector such that it satisfies Lorentz symmetry. Then the deliberately chosen conformally flat hypersurface guarantees that the Lie derivatives of the Killing vectors must be proportional to the Lorentz transformation Killing vectors $J^{\mu\nu}$:

$$\hat{x}^\mu = ia\left(k_4\frac{\partial}{\partial k_\mu} + k^\mu\frac{\partial}{\partial k_4}\right) , \tag{6.2}$$

$$[\hat{x}^\mu, \hat{x}^\nu] = ia^2\hat{J}^{\mu\nu} = -a^2\left(k^\mu\frac{\partial}{\partial k_\nu} - k^\nu\frac{\partial}{\partial k_\mu}\right) , \tag{6.3}$$

where $k^\mu = \eta^{\mu\nu}k_\nu$, $\eta^{\mu\nu}$ is the 4-d Minkowski metric and $[\ ,\ ]$ is the commutator. The momentum coordinate is the exponential map,

$$\hat{p}_\mu = a^{-1}k_\mu/k_4 \,, \tag{6.4}$$

on which the Lorentz transformation Killing vectors $\hat{J}^{\mu\nu}$ locally have the same form as the traditional Lorentz transformation generators $\hat{J}^{\mu\nu} = \hat{x}^\mu\hat{p}^\nu - \hat{x}^\nu\hat{p}^\mu$. Snyder's approach therefore can be viewed as a non-abelian realization of the Lorentz group. The Heisenberg relation and the uncertainty relation are twisted accordingly to be

$$[\hat{x}^\mu, \hat{p}_\nu] = i\left(\delta^\mu_\nu - a^2\eta^{\mu\lambda}\hat{p}_\lambda\hat{p}_\nu\right) , \tag{6.5}$$

$$\Delta x^\mu\Delta p_\nu \geq \frac{1}{2}\left(\delta^\mu_\nu - a^2\eta^{\mu\lambda}\left\langle\hat{p}_\lambda\hat{p}_\nu\right\rangle\right) . \tag{6.6}$$

As we will see in sec.7.4, our own version of quantized spacetime carries the same uncertainty relation as Snyder's up to the first order in p^2.

An weaker deformation, called κ-Poincaré group, later invoked by G. Amelino-Camelia [15, 13] for the doubly special relativity, was first introduced by S. Majid and H. Ruegg [12] as follows:

$$\left[x^i, x^j\right] = 0\,, \quad \left[x^i, x^0\right] = \kappa^{-1}x^i\,, \quad [p_\mu, p_\nu] = 0\,. \tag{6.7}$$

This system can be regarded as an $AdS_3 \times \mathbb{R}^{1,0}$ hypersurface in a 5-d momentum space, where an upper bound κ for the spatial momentum $|\vec{p}|$ served as a cutoff scale for the QFT built on top of it. The realization of a maximally symmetric momentum space and the flat p_0 direction implies a vanilla Lorentz group constructed from $\hat{p}\hat{x}$ and a linear action on p_0. Note, however, that the cylindrical structure implies a non-linear Lorentz boost N_i on the spatial momentum

$$[N_i, p_j] = i\delta_{ij}\left[\frac{\kappa}{2}\left(1 - e^{-2p_0/\kappa}\right) + \left|\frac{\vec{p}}{2}\right|^2\right] - \frac{i}{\kappa}p_i p_j \,. \tag{6.8}$$

A maximally achievable spatial momentum κ therefore corresponds to an infinite energy p_0. In sec.7.4 , we will demonstrate that there also exists a maximal spatial momentum with finite energy in our theory. However, their commutation relation and accordingly their generalized uncertainty relation, share no similarity to our result.

6.2 Angular Momentum Space and $U(\mathfrak{su}(2))$ algebra

Another work that is closely related to what we propose here is the angular momentum space theory introduced by Shahn Majid [18], where the group structure of the angular momentum operator, $SU(2)$, is considered as a deformation of the 3-d spacetime

$$\left[x^i, x^j\right] = 2i\lambda\epsilon^{ij}_{k}x^k \,. \tag{6.9}$$

The most surprising feature of this theory is that the construction of the differential structure through C^* algebra implies the existence of a fourth direction, which supposedly is the time. Assuming the completeness of the Lie algebra, the commutation relation of the 1-form and the exterior derivative of the Fourier mode are

$$[x_i, dx_j] = i\lambda\epsilon_{ijk}dx_k + \lambda\delta_{ij}d\tau \,,\; [x_i, d\tau] = \lambda dx_i \tag{6.10}$$

$$de^{ik\cdot x} = \left[\frac{i\sin(\lambda k)}{\lambda k}k\cdot dx - \frac{8d\tau}{\lambda}\sin^2\left(\frac{\lambda k}{2}\right)\right]e^{ik\cdot x} \tag{6.11}$$

where d stands for the exterior derivative, $dx_i = \sigma_i/2$ and $d\tau = I_2/2$, σ_i are the Pauli matrices, I_2 is the identity operator, k is the Fourier momentum with $k^2 = k_a k^a$, and $k \cdot x = k_a x^a$. Majid regarded this theory as a 3-d remnant of q-deformed poincaré group theory [24]. We will show that what we propose is another way of extending the theory to 4-d, by regarding $SU(2)$ group as Clifford algebra on 3-d Euclidean manifold, or by focusing on connected subgroup of the $Spin(3,1)$.

6.3 Adler's Spinorial Spacetime

Following a completely different reasoning, R. Adler arrived at a quantized spacetime as follows. Considering the Riemannian distance functional $ds_R^2 = g_{\mu\nu} dx^\mu dx^\nu$, a natural way to get the operator spectrum, other than the spectral square root [26], would be via Clifford algebra. One then obtains a linear functional $ds_L = \gamma_\mu dx^\mu$ connecting the coordinate difference to the linear line element. The prize to pay is that the new transfer functional γ_μ, which was chosen to be the chiral gamma matrix, is a matrix instead of a pure number.

To compensate that, Adler reinterprets the distance functional as a QM object, called "linear line element operator", whose eigenvalue is the proper distance and the state describes an eigen-direction along which the performed measure is completely certain.

$$ds_A = \langle \hat{ds} \rangle = \langle \epsilon \, | \gamma_\mu dx^\mu | \, \epsilon \rangle = \epsilon_\mu dx^\mu \, , \tag{6.12}$$

$$\langle \epsilon \, | | \, \epsilon \rangle = (|\epsilon\rangle)^\dagger \, |\epsilon\rangle = 1 \, , \tag{6.13}$$

where $\hat{ds}$ stands for the linear line element operator, γ_μ are the chiral gamma matrices, and ϵ_μ is the expectation value of the distance functional. The subscript A in ds_A indicates that this is Adler's version of line element. In addition, Adler assumes that the traditional picture of the infinitely differentiable manifold should be replaced by a piecewise-linear manifold with the curve length

$$L_C = \sum_i \left\langle \hat{\Delta s} \right\rangle_{(i)} = \sum_i \left\langle \epsilon_{(i)} \right| \gamma_\mu \Delta x^\mu_{(i)} \left| \epsilon_{(i)} \right\rangle \, , \tag{6.14}$$

where (i) indicates the site and $\Delta x = \lambda dx$ is the discrete coordinate difference. So instead of the Killing vector of a curved momentum space serving as the coordinate measure or a twisted commutation relation of position operator, the proper distance is treated as the addition of generators of the spin group on classical x-space, similar to the 't HOOFT operator on a spacetime lattice.

This theory introduces an uncertainty to the proper distance measure as

$$\Delta L_C^2 = \sum_i \left[1 - \left(\dot{x}^{\mu(i)} \epsilon_{\mu(i)} \right)^2 \right] g_{\mu\nu} \Delta x^\mu_{(i)} \Delta x^\nu_{(i)} \, , \tag{6.15}$$

where $\dot{x}^\mu = dx^\mu / ds$ is the 4-velocity, and ϵ_μ is the preferred direction that minimizes the uncertainty. The notion of a preferred direction inevitably breaks the Lorentz invariance, unless the theory is non-dissipative or is at high temperature limit. The whole purpose of using Clifford algebra, to preserve Lorentz invariance, is therefore defeated. The failure of Adler's original attempt promotes us to construct a different realization of the same idea.

Chapter 7

Spinorial Spacetime

7.1 Reinterpretation, Reformulation and Correction to Adler's Proposal

Following Adler's argument, the Riemannian line element $ds_R^2 = g_{\mu\nu}dx^\mu dx^\nu$ can be discretized and factorized via the measurement of the square of the linear line element

$$\Delta s_A^2 = \left\langle \widehat{\Delta s^2} \right\rangle = \langle \epsilon \left| \gamma_\mu \Delta x^\mu \gamma_\nu \Delta x^\nu \right| \epsilon \rangle \ , \tag{7.1}$$

with

$$\left\{ \gamma^I , \gamma^J \right\}_{pq} = 2\eta^{IJ} \otimes I_{pq} \, , \tag{7.2}$$

$$\left[\gamma^I , \gamma^J \right]_{pq} = -2i\sigma^{IJ}_{pq} \, , \tag{7.3}$$

$$\gamma^\mu = e^\mu_I \gamma^I \, , \tag{7.4}$$

$$g_{\mu\nu} = \eta_{IJ} e^I_\mu e^J_\nu , \eta_{IJ} = g^{\mu\nu} e^I_\mu e^J_\nu \, , \tag{7.5}$$

where e is the tetrad field and $\{ \ , \ \}$ is the anti-commutator.

Care must be taken when one deals with the definition and the interpretation of the measure. In Adler's approach, Eq.(6.13) was used to define the braket, while Eq.(6.12) was interpreted as a distance functional. However, this choice suffers some drawbacks and is unsuitable for the construction of our quantum spacetime theory.

First, the linear line element operator contains the exact information one would expect to be hidden inside the Hilbert space of the quantized spacetime, i.e., the direction. In the original interpretation, the Hilbert space contains the information for the uncertainty of distance measurement rather than the direction itself. The direction of the line element is provided externally in Eq.(6.12) since the theory is describing a quantized distance functional, rather than a quantized spacetime. The existence of a favored direction that minimizes the uncertainty also breaks Lorentz invariance and isotropy at the smallest scale. The salient feature of Lorentz symmetry in Adler's theory (Dirac's way of taking square root clearly is Lorentz invariant) is therefore lost.

Second, when one measures the proper distance of null eigenstates (which should be quite common given the fact that all particles are massless prior to electro-weak symmetry breaking) along any direction, because of the choice of normalization the proper distance would always be zero. So for a null state even if the curve is not along null direction the proper distance would still be null. To wit, the measure of proper distance is completely uncertain for a non-null displacement on a null state.

Third, the outcome of the linear distance functional depends heavily on the choice of the representation of the Clifford algebra. A complex representation could result in a complex proper distance, which is a radical departure from usual GR. Although Adler tries to address this issue by fixing the representation, the problem still exists as long as the proper distance, being a physical measure, is not a scalar of Clifford algebra, i.e. not representation independent.

Clearly, these observations indicate the necessity of reinterpretation of Adler's linear line element and a new choice of normalization. We look for new definition that should satisfy Lorentz symmetry, should not have preferred direction, should produce reasonable results for null states, and should be independent of the choice of the representation.

So we give up Eq. (6.13) and introduce a new operator $\Delta\hat{X}^I$, called "spacetime interval operator":

$$\Delta\hat{X}^I = e^I_\mu \Delta\hat{X}^\mu = \lambda\gamma^I \,, \tag{7.6}$$

$$\left\langle \Delta\hat{X}^I \right\rangle = \bar{\psi}\Delta\hat{X}^I\psi = \psi^\dagger\gamma^0\Delta\hat{X}^I\psi \,, \tag{7.7}$$

$$\bar{\psi}\psi = \begin{cases} 1 & , \ \forall \text{ time-like states} \\ 0 & , \ \forall \text{ null states} \\ -1 & , \ \forall \text{ space-like states} \end{cases} \tag{7.8}$$

$$\bar{\psi}\gamma^I\psi = \begin{cases} n^I & , \ \forall \text{ non-null states} \\ k^I & , \ \forall \text{ null states} \end{cases} \tag{7.9}$$

$$ds^2 = \eta_{IJ} \left\langle \Delta\hat{X}^I \Delta\hat{X}^J \right\rangle = 4\lambda^2\bar{\psi}\psi \,. \tag{7.10}$$

Here λ is the characteristic length of the quantized spacetime that is of the order of Planck length and will be derived in sec.7.2, n^I is a non-null vector with $n_I n^I = \pm 1$, and k^I is a null vector with positive k^0. The appearance of the γ^0, and the choice of normalization can be appreciated by looking at the solution of Dirac field equation (See, for example, Ch. 3-3 of Peskin & Schroeder [27].) Physically the insertion of γ^0 makes the normalization condition Lorentz invariant, and for the massless case the choice of normalization is equivalent to the introduction of the foliation along the time coordinate.

	$\Delta\vec{X}$	ΔV_3	$\Delta\vec{V}$	Δt	Δs^2	$\Delta\vec{A}$	$\Delta\vec{A}_t$	ΔV_4
$\Delta\vec{X}$	O	O	O	O	X	X	X	X
ΔV_3	O	O	O	O	X	X	X	X
$\Delta\vec{V}$	O	O	O	O	O	O	O	O
Δt	O	O	O	O	O	O	O	O
Δs^2	X	X	O	O	O	O	X	X
$\Delta\vec{A}$	X	X	O	O	O	O	X	X
$\Delta\vec{A}_t$	X	X	O	O	X	X	O	O
ΔV_4	X	X	O	O	X	X	O	O

Table 7.1: A commutativity table showing possible ways of labelling Hilbert space. For elements T_{mn} inside the table, "O" means m-th basis commutes with n-th basis, and "X" means non-commutativity. Here all vectors are along spatial eigen-direction $n^i = \langle\Delta X^i\rangle$, and $\Delta\vec{X} = n_i\Delta X^i$ is the spatial interval, $\Delta V_3 = \Delta X^1\Delta X^2\Delta X^3$ is the time-like 3-volume, $\Delta\vec{V} = -n_i\epsilon^i_{jk}\Delta X^0\Delta X^j\Delta X^k$ is the spatial 3-volume, Δt is the time difference, Δs^2 is the proper distance square, $\Delta\vec{A} = n_i\epsilon^i_{jk}\Delta X^j\Delta X^k$ is the spatial area, $\Delta\vec{A}_t = n_i\Delta X^0\Delta X^i$ is the time-like area, and $\Delta V_4 = \Delta X^0\Delta X^1\Delta X^2\Delta X^3$ is the 4-volume. Notice that actually $\vec{V}$ can always be described by products of two non-trivial quantum numbers in the system.

This new measurement is not a distance measure at all, but a local spacetime interval operation on the exponential map of Riemann Normal Coordinate. One should not misinterpret the operator as a coordinate difference operator, since it actually lies on the tangent bundle of the manifold. A better way to understand it is to treat it as a discretized version of the velocity 4-vector. And only when combined with the tetrad does the coordinate difference measure $\Delta\hat{X}^{\mu}$ reappear.

Just like the components of a vector in GR, $\Delta\hat{X}^{I}$ (gamma matrices) are not physical objects. To measure the velocity of a particle we need two-particle interaction, and the physical object is the inner product $r_I\Delta\hat{X}^{I}$, where r_I is the classical trajectory of a probe particle expressed in the same representation as $\Delta\hat{X}^{I}$. No matter what representation of Clifford algebra we are choosing, the measurement is always a scalar. Therefore all the derivations and results we obtained are representation independent. The only exception is that in sec. 6 we require the realness of $\Delta\hat{X}^{I}$ during derivation of GUP. However one should get the same GUP regardless of the representation used.

The new choice of interpretation also implies the existence of an underlying minimal distance. Due to the special structure of Clifford algebra, one can immediately obtain $\left|\left\langle \Delta X^{I}\Delta X^{I}\right\rangle\right| = \lambda^2$ for non-null cases and 0 for null cases, implying that there are uncertainties within the spacetime interval measurement similar to what was obtained in Ref.[22], where the uncertainty lies on proper distance measurement. But in our case even such uncertainties are Lorentz invariant. One may try to obtain the variance of interval measure:

$$
\begin{aligned}
\left\langle \mathrm{var}\left(r_I\Delta X^{I}\right)\right\rangle &= \left|\left\langle \left(r_I\Delta X^{I}\right)^2\right\rangle - \left\langle r_I\Delta X^{I}\right\rangle^2\right| \\
&= \lambda^2\left|r\cdot r\times n\cdot n-(r\cdot n)^2\right| , \qquad (7.11)\\
\left\langle \mathrm{var}\left(\Delta s\right)\right\rangle &= \left|\left\langle \Delta X^{I}\Delta X_{I}\right\rangle - \left\langle \Delta X^{I}\right\rangle\left\langle \Delta X_{I}\right\rangle\right| \\
&= \begin{cases} 3\lambda^2 & ,\ \forall \text{ non-null states} \\ 0 & ,\ \forall \text{ null states} \end{cases} \qquad (7.12)
\end{aligned}
$$

Here $n^I = \left\langle \Delta X^{I}\right\rangle$, r^I is the ruler, and $A\cdot B = \eta_{IJ}A^I B^J$ is the inner product. Clearly along eigen-direction there is no uncertainty at all since it is the direction where eigenstates are defined. However along the transverse direction the measurement is completely uncertain. From this point of view the behaviour of the spacetime interval operator is exactly the same as spin operators in relativistic QM. They both have 3 definite quantum numbers, i.e., $S^2/\Delta t$, $\vec{S}/\Delta\vec{X}$ along spatial eigen-direction, and helicity/ΔV_3, where ΔV_3 is the spatial 3-volume. There are also other possible ways of labelling Hilbert space, which are shown in Table 7.1.

Naïvely, in $SO(3,1)$ system there are 4 quantum numbers: the 4-momentum. However they do not correspond to the quantum numbers in our theory since the momentum operators do not commute with each other. Only at the decoherence limit will the additional 4 quantities, eigen-direction, spatial 3-volume along eigen-direction and proper distance, emerge.

An important feature of Adler's original interpretation is that the proper time difference $\Delta s \propto \gamma^\mu$ can have two eigenvalues of same magnitude but opposite sign. Therefore in his theory it is permissible to move backward in time, zigzag around the same spot at high temperature if no rule forbids the excitation of these states. However in our interpretation, time difference is now proportional to the identity operator due to the choice of measure, rendering its expectation value positive definite. Thus arrow of time problem is perfectly solved without invoking second law of thermodynamics.

In Ref.[22], Adler suggests that one may take these tiny line elements as building blocks of a curve, without specifying what kind of curve it is. Since in the original paper the measurement of linear line element operators are associated with $SO(3,1)$ proper distance, this curve resembles a geodesic, called "quantized geodesic" due to its discrete nature. Under our spacetime interval operators, the link to the geodesic becomes more explicit since a trajectory is specified along the geodesic as

$$|\mathcal{C}\rangle = \bigoplus_i \left|n_{(i)}\right\rangle,\ n^I_{(i)} = \left\langle n_{(i)}\right| \Delta X^I \left|n_{(i)}\right\rangle \,, \tag{7.13}$$

$$X^\mu_{(i)} = \sum_{j=1}^{i} e^\mu_{I(j)} n^I_{(i)},\ s = \sum_i \sqrt{n^I_{(i)} n_{I(i)}} \,. \tag{7.14}$$

Here $|\mathcal{C}\rangle$ is the composite state for geodesic, and (i) indicates the i-th site along the geodesic. Following usual convention in special relativity, positive eigenvalue of proper distance $\Delta s = \pm\sqrt{\Delta s^2}$ is chosen due to the positivity of time difference.

7.2 Obtainbing Action Through Fermionization

Up until now our theory is still presented in a schematic way where the operators and the measure were not derived from first principles. Given Eq.(7.7), we can deduce that a worldline action in terms of bi-fermionic fields exhibiting bosonic behavior should describe our theory. A natural tool to attain this action would be the bosonization in 2-d QFT [28]. By considering the worldline as the low energy limit of a cylindrical worldsheet, we may apply the fermionization on the worldsheet action and compactify it back to 1-d.

Considering the worldline action for a relativistic particle

$$S_R = \int \left(\xi g_{\mu\nu} \frac{dX^\mu}{d\tau} \frac{dX^\nu}{d\tau} - \frac{m^2}{2\xi} \right) d\tau \,, \tag{7.15}$$

doi:10.6342/NTU201603461

where τ is a parameter along the particle trajectory, and ξ is an axillary field with equation of motion

$$\xi = m\left(g_{\mu\nu}\frac{dX^\mu}{d\tau}\frac{dX^\nu}{d\tau}\right)^{-1/2} . \tag{7.16}$$

One can describe it as the Kaluza-Klein ground state of the worldsheet Polyakov action on a cylinder through compactification along small perimeter $L \ll m$

$$S_R \approx \int_0^L d\sigma^1 \frac{S_R + c(\sigma^1)}{L} \approx S_P\,, \tag{7.17}$$

$$S_P = \frac{1}{8\pi l_s^2}\int d^2\sigma\sqrt{-h}h^{\alpha\beta}g_{\mu\nu}\partial_\alpha X^\mu \partial_\beta X^\nu\,, \tag{7.18}$$

where $l_s = \sqrt{L/\left(4\pi m\right)}$ is the string length, $\sigma^0 = \tau$, and σ^1 is the compactified direction. Up to now we still cannot apply the fermionization. A naïvely fermionized action would be ambiguous as the group structure of the system $g\left(X\right)$ is still undetermined. To avoid such problem one may rely on tetrad formalism to pull g back to Minkowski metric η and obtain a $SO\left(3,1\right)$ theory

$$S_P = \frac{1}{8\pi l_s^2}\int d^2\sigma\sqrt{-h}h^{\alpha\beta}\nabla^I_{K\alpha}X^K\nabla_{IL\beta}X^L\,, \tag{7.19}$$

$$X^I = e^I_\mu X^\mu\,,\ \nabla_\alpha = \partial_\alpha + \omega^I_{J\alpha} - \Gamma^I_{J\alpha}\,, \tag{7.20}$$

where the tetrad field e should be a functional of X, ∇_α is the covariant derivative which annihilates the tetrad $\nabla_\alpha e = 0$, $\omega^I_{J\alpha}$ is the antisymmetric spin connection, and $\Gamma^I_{J\alpha}$ is the symmetric affine connection. The $SO\left(3,1\right)$ spacetime group can now be replaced with the $Spin\left(3,1\right)$ group, making this theory a spacetime bi-fermion theory. The new action under the gauge condition $\Gamma^I_{I\alpha} = 0$ would be

$$S_{Spin} = \frac{1}{8\pi}\int d^2\sigma\sqrt{-h}D_\alpha\not{\chi}D^\alpha\not{\chi}\,, \tag{7.21}$$

$$D_\alpha\not{\chi} = l_s^{-1}\gamma_I e^I_\mu \partial_\alpha X^\mu\,,\ \not{\chi} = l_s^{-1}\gamma_I e^I_\mu X^\mu\,, \tag{7.22}$$

$$D_\alpha = \partial_\alpha + \frac{1}{2}\omega^I_{J\alpha}\left[\gamma_I,\gamma^J\right] = \partial_\alpha - i\omega^I_{J\alpha}\sigma^J_I\,, \tag{7.23}$$

where $\not{A} = \gamma_I A^I$ and $D_\alpha\not{\chi}$ is the generalized velocity of the $Spin\left(3,1\right)$-valued worldsheet scalar $\not{\chi}$ of dimension $[m^0]$. Notice that $D_0\not{\chi}$ is exactly the continuum limit of Adler's linear line element operator, indicating that we are on the right track. Since the mapping from worldsheet space to $Spin\left(3,1\right)$ space is trivial for K-K ground state, both E. Witten's approach [29] and Steinhardt's [30] preserve the symmetry after fermionization. Therefore one can fermionize the theory by checking the bozonization dictionary:

$$4\pi\bar{\eta}\left(1\pm\sigma^2\right)\eta \Longleftrightarrow e^{\pm 4\pi i\phi} \tag{7.24}$$

$$\bar{\eta}\sigma^\alpha\eta \Longleftrightarrow -2\epsilon^{\alpha\beta}D_\beta\phi \tag{7.25}$$

$$i\bar{\eta}\sigma^\alpha D_\alpha\eta \Longleftrightarrow D_\alpha\phi D^\alpha\phi \tag{7.26}$$

, where ϕ is a real scalar of dimension $[m^0]$, η is a 2-d worldsheet Majorana spinor of dimension $[m^0]$, σ^α are the 1+1-d Majorana-Weyl matrices , and $\sigma^2 = \sigma^0\sigma^1$. For the sake of simplicity we have rescaled both η and ϕ by a factor of $\sqrt{4\pi}$. Applying these rules to Eq.(7.21) one arrives at

$$S_F = \int d^2\sigma\sqrt{-h}\left(i\bar{c}\sigma^\alpha D_\alpha c\right) \,, \tag{7.27}$$

where c is a 4-d spacetime spinor valued 2-d worldsheet Majorana-Weyl spinor.

From constraints of the K-K ground state and the bosonization dictionary one immediately obtains

$$D_1\not\chi = 0 = -\frac{1}{2}c^\dagger c \,, \tag{7.28}$$

$$D_0\not\chi = \not v = \frac{1}{2}c^\dagger\sigma^2 c \,, \tag{7.29}$$

where $\not v$ is the velocity. To satisfy these two requirements the only possible solution would be

$$c = (\psi, \psi C) = \left(\sqrt{\gamma^0\not v}\psi_0, \sqrt{\gamma^0\not v}\psi_0 C\right) \,, \tag{7.30}$$

where ψ_0 is a normalized spinor with $\psi_0^\dagger\psi_0 = 1$, and C is the usual hermitian charge conjugation operator that transforms $\bar\psi\gamma^\mu\psi$ to $-\bar\psi\gamma^\mu\psi$. Finally we can obtain the compactified action and the geodesic equation in terms of fermionic field ψ

$$S_C = \int d\tau\left(i\bar\psi D_0\psi\right) \,, \tag{7.31}$$

$$\frac{d^2X^\mu}{d\tau^2} = \frac{d}{d\tau}\bar\psi e_I^\mu\gamma^I\psi = -e_I^\mu\Gamma^I_{J0}v^J \,. \tag{7.32}$$

Since the worldsheet spinor $\bar{c}c$ is conserved, from Eq.(7.24) and the identity

$$e^{i\not F} = \cos\left(\sqrt{F_IF^I}\right)I_4 + i\sin\left(\sqrt{F_IF^I}\right)\not F \,, \tag{7.33}$$

we obtain

$$\not\chi = \left(\frac{n}{2\sqrt{|v^2|}} + q\right)\not v \quad , \; n \in \mathbb{Z} \,, \tag{7.34}$$

where $v^2 = v_Iv^I$, q is a scalar constant in terms of v^2, and spacetime is quantized accordingly with the characteristic length

$$\lambda = \frac{1}{2}l_s \,. \tag{7.35}$$

Eqs.(7.7) to (7.9) can be re-derived respectively as

$$\left\langle\Delta\hat{X}^\mu\right\rangle = \lambda\bar\psi\gamma^\mu\psi = \frac{\lambda}{4}tr\left(\gamma^\mu\not v\right) = \lambda v^\mu \,, \tag{7.36}$$

$$v^2 = \frac{\left|\left\langle\Delta\hat{X}^\mu\right\rangle\right|^2}{\lambda^2} \approx 4\Delta\not\chi\Delta\not\chi = \frac{v^2}{|v^2|} = \text{sign}\left(v^2\right) \,, \tag{7.37}$$

$$\bar\psi\psi = \frac{\lambda}{4}tr\left(\not v\right) = 0 \,. \tag{7.38}$$

doi:10.6342/NTU201603461

Since in this section we focus on eigenstates of the spacetime interval operator $\Delta\hat{X}^I$, $\bar{\psi}\psi$ must vanish. If the constraint Eq.(7.29) is substituted with $\bar{\psi}\psi = const.$, from Eq.(7.24) and (7.33) we immediately obtain

$$\bar{\psi}\psi = 1 \vee 0 \vee -1 \; . \tag{7.39}$$

Therefore we show that the quantization scheme introduced in sec.7.1 can be reproduced explicitly.

A phenomenological effective action is proposed by Adler [22] as

$$H_{eff} = E_f \sum_i \epsilon^{\mu(i)} \gamma_{\mu(i)} \; , \tag{7.40}$$

where ϵ^μ is the preferred direction and (i) indicates the site. This action is problematic not only because it has a preferred direction, but also because the propagator of the associated particles would be a tadpole since the action is linear in X^μ. This problem is solved naturally in our theory since we write down the action directly by fermionizing the worldline action with an usual p^{-2} propagator.

7.3 Composite and Holographic Nature of the Spacetime

Following the same idea presented at the end of sec.III, we can finally define the position operator and the position eigenstate. Since

$$\langle X^\mu \rangle = \sum_i \left\langle e^\mu_I \Delta X^I \right\rangle_{(i)} \; , \tag{7.41}$$

one can obtain the form of $\hat{X}^\mu$ and its eigenstate $|x\rangle$:

$$\hat{X}^\mu = \lambda \sum_i \left(e^\mu_I \gamma^I_{(i)} \underset{j<i}{\otimes} \gamma^0_{(j)} \right) \; , \tag{7.42}$$

$$|x\rangle = \underset{i}{\oplus} \left| \Delta x_{(i)} \right\rangle \; , \tag{7.43}$$

where $\otimes$ is the direct product, $\underset{i}{\oplus}$ and $\underset{i}{\otimes}$ are the direct sum and the direct product over sites with dummy index i. The occurrence of γ^0 in the off-site part is purely artificial, and can be removed by choosing other representations, e.g. $\hat{X}^\mu = \sum \lambda \bar{\psi}_{(i)} e^\mu_I \gamma^I \psi_{(i)}$. The position operator can be envisioned as the 't HOOFT operator on a 1-D spin chain, and the associated Fourier transformation operator $e^{ik_\mu X^\mu}$ as the Wilson line operator. This kind of visualization is inherited from the bozonization.

Considering the fact that the commutator of position operator is vanishing at large scale, the spacetime interval operators of different sites should commute as long as they are far apart from each other. The simplest assumption would be

$$\left[\gamma^I_{(i)}, \gamma^J_{(j)} \right] = 0. \tag{7.44}$$

The structure of the spacetime interval operator under this assumption resembles the spin operators in the 4-d Heisenberg model, which is also classical in exterior space but fermionic on site. Notice that the dynamics of the Heisenberg model is completely determined by the Hamiltonian and the commutation relation between nearest neighbors, so does our theory. The assumption we made therefore is equivalent to turning off the non-local dynamics of null geodesic. This makes the structure of the theory greatly simplified, but still provides sufficient insight to the properties of the position operator and the spacetime itself. It is now straightforward to derive the commutation and anti-commutation relations:

$$
\begin{aligned}
\frac{1}{2\lambda^2}\left[\hat{X}^\mu,\hat{X}^\nu\right] &= i\sum_i \left(\sigma^{\mu\nu}_{(i)} \underset{j\neq i}{\otimes} I_{(j)}\right)\,, && (7.45)\\
\frac{1}{2\lambda^2}\left\{\hat{X}^\mu,\hat{X}^\nu\right\} &= \sum_i g^{\mu\nu}_{(i)}\left(\underset{j}{\otimes} I_{(j)}\right) \\
&\quad + \sum_{i,j\neq i}\left(\gamma^\mu_{(i)}\otimes\gamma^\nu_{(j)} \underset{i\neq q\neq j}{\otimes} I_{(q)}\right)\,, && (7.46)\\
\frac{1}{2}\left\langle\left\{\hat{X}^\mu,\hat{X}^\nu\right\}\right\rangle &= \left\langle\hat{X}^\mu\right\rangle\left\langle\hat{X}^\nu\right\rangle + \sum_i \Big(\lambda^2 g^{\mu\nu} \\
&\quad - \left\langle\Delta X^\mu\right\rangle_{(i)}\left\langle\Delta X^\nu\right\rangle_{(i)}\Big)\,, && (7.47)
\end{aligned}
$$

where $\underset{i\neq q\neq j}{\otimes} I_{(q)}$ is the direct product over all sites except the i-th site and the j-th site. At the large scale limit these relations match the classical results. Non-classical parts of both the anti-commutator and the commutator are of the order of λX. The physical quantity corresponding to these corrections are basically the sum of the "surface area" of the discrete spacetime along the curve linking from the origin to the point X. It is clear that the spacetime in this work, contrary to those of most other theories, is neither commutative nor anti-commutative.

Another important aspect of non-commutativity of spacetime is the holographic nature of our theory. Since the position eigenstates are composite, there are only $(N+1)^2$ distinguishable and physically acceptable configurations for states composed by N line elements. A 2-line-element state resembles a composite spin-1 particle, with the proper distance and the area quantum number of the former corresponding to the charge and the spin of the latter, respectively, both with quantum numbers 1, 0, or -1. Therefore it is with no doubt that only $\mathcal{O}\left(N^3\right)$ different states are allowed within a 4-sphere, implying that the spacetime information can be written in a 3-dimensional quantum language. With the equation of motion in Eq.(7.32), the degree of freedom, or entropy, is proportional to surface area of the system.

7.4 Generalized Uncertainty Principle

In QM, one can define a translation operator $\hat{T}\left(\epsilon\right)$ in terms of the momentum operator:

$$\hat{T}_\mu\left(\epsilon\right) = e^{-i\epsilon\hat{P}_\mu}\,, \tag{7.48}$$

which satisfies the commutation relations

$$\left[\hat{X}^\mu, \hat{T}_\nu\left(\epsilon\right)\right] = \epsilon\,\delta^\mu_\nu \hat{T}_\mu\left(\epsilon\right)\,, \tag{7.49}$$

$$\left[\hat{T}_\mu, \hat{T}_\nu\right] = 0\,. \tag{7.50}$$

Clearly as long as the inversion of the exponential operator exists, one can reversely construct the momentum operator in terms of the translation operator defined above:

$$\hat{P}_\mu = i\epsilon \ln\left(\hat{T}_\mu\left(\epsilon\right)\right)\,, \tag{7.51}$$

$$\begin{aligned}\left[\hat{X}^\mu, \hat{P}_\nu\right] &= \left[\hat{X}_\mu, i\epsilon\ln\left(\hat{T}_\nu\left(\epsilon\right)\right)\right] \\ &= i\epsilon\hat{T}_\mu(\epsilon)\frac{\partial\ln\left(\hat{T}_\nu(\epsilon)\right)}{\partial\hat{T}_\mu(\epsilon)} = i\delta^\mu_\nu\,,\end{aligned} \tag{7.52}$$

$$\left[\hat{P}_\mu, \hat{P}_\nu\right] = 0\,. \tag{7.53}$$

So instead of defining the momentum operator directly, we choose to define the eigenstate of the translation operator, a.k.a. the plane wave solution, for it is less ambiguous, more visualizable, and easier to define.

Since the time direction has nothing to do with our topic of interest (GUP) for the moment, for the sake of simplicity, we will restrict the system to a simpler one with the existence of foliation and invoke ADM formalism to reduce the symmetry down to $Spin(3)$. The system can be understood as a spin chain in the zero temperature limit, with the coordinate measure being the total spin. This system can be reinterpreted as a bosonic system with SU(2) symmetry even at the quantum level, as demonstrated in the non-abelian bosonization. A naïve guess from QM is that the total spin operator, or the spatial coordinate operator, is now a SU(2) operator of all representations. One can therefore regard this system as exactly the same one in Ref.[18]. As shown in Eqs.(6.9) to (6.11), an immediate conclusion would be the existence of an exterior derivative that can be treated as a momentum operator:

$$\begin{aligned}p_i &= dx_i\tilde{p}_i \equiv -idx_i\left(dx_i\cdot de^{ik\cdot x}\right)e^{-ik\cdot x} \\ &= \left(\lambda k\right)^{-1}\sin\left(\lambda k\right)k_i dx_i\,,\end{aligned} \tag{7.54}$$

$$[x_i, p_j] = i\delta_{ij}dx_j + i\lambda\epsilon_{ijk}dx_k\tilde{p}_j + \lambda\delta_{ij}d\tau\,\tilde{p}_j\,, \tag{7.55}$$

$$[p_i, p_j] = i\epsilon_{ijk}dx_k\tilde{p}_i\tilde{p}_j\,, \tag{7.56}$$

where p_i is the projected momentum that generates translation along x_i, and $\tilde{p}_i$ is its 1-form component.

One can therefore compute the uncertainty relation through

$$\begin{aligned}\Delta x_i \Delta p_j \geq \frac{1}{2}\Big[& \left\langle [x_i, p_j] \right\rangle^2 \\ & + \big(\left\langle \{x_i, p_j\} \right\rangle - 2 \left\langle x_i \right\rangle \left\langle p_j \right\rangle \big)^2 \Big]^{1/2} . \end{aligned} \tag{7.57}$$

In the low momentum limit ($\langle k \rangle$ small and $\langle x \rangle \to 0$), we obtain

$$\Delta x_i \Delta p_j \geqslant \frac{1}{2}\left(\delta_{ij} + 2\lambda^2 \delta_{ij} \left\langle k_i \right\rangle \left\langle k_j \right\rangle \right) . \tag{7.58}$$

The GUP of our theory is of the usual form. (e.g., Snyder's GUP in Eq.(6.6) is identical to ours with relation $\lambda = \sqrt{2}a$)

7.5 Smearing Effect

It is straightforward to apply the quantized geodesic obtained in Sec.7.3 to trajectories of cosmic rays, which may serve as an astrophysical test for this theory through the smearing of particle trajectory. Consider, for example, the null geodesic of a 10 MeV photon emitted from a gamma ray burst afterglow at high redshift ($z \approx 10$). Because the Lorentz invariance is manifest in our theory, the smearing effect occurs only along the perpendicular direction. Assuming Gaussian distribution of photons at source, we find, from Eq.(7.11) and Eq.(7.12), that the smearing of the photon is of the order of $\sqrt{E\lambda^2 \, d_S\,(z \approx 10)} \approx 10^{-14}\lambda$ meter, where $d_S = \int_0^z \frac{(1+z')dz'}{H(z')}$ is the rescaled distance taking the rescaling of the variance into account, E is the GRB characteristic energy, and λ is the scale of our theory in the unit of the Planck length. Clearly it is impossible to identity such tiny effect in the near future.

Let us consider an EeV neutrino at high redshift ($z \approx 10$) as another example. The smearing for massive particles along the perpendicular direction is of the order of $\sqrt{\frac{E}{m_\nu}\lambda \, d_S\,(z \approx 10)} \approx 100\sqrt{\lambda}$ meter. For time-like geodesic, in addition to perpendicular direction, there are also variance in proper distance, which allow us for more precise measurement. The smearing is at most $\sqrt{3\lambda t_P \, T\,(z \approx 10)} \approx \sqrt{\lambda}$ picosecond, where t_P is the Planck time and T is the time taken from $z = 10$ to $z = 0$. One possible way to probe the smearing of the arrival time is by observing both neutrinos and gravitational waves from a single merger event of the black hole-neutron star binary. Since typically the neutrino flux bumps up sharply 0.5 ms after the merger event [31], a time-resolution of 0.5 ms can be achieved by detecting neutrinos right after the detection of the gravitational merger event. The resolution of λ is therefore of the order 10^{-17} meter. An improvement on the simulation could possibly enhance the time-resolution in this merger scenario and allow a tighter constraint on the value of λ.

doi:10.6342/NTU201603461

Chapter 8

Conclusion and Future Work

8.1 Macroscopic Universe

It is still very hard to draw any conclusion from the preliminary result, but at least it is very clear that indeed a local inhomogeneity can explain some parts of the tension of H_0 between local SNe measurement and CMB measurement. We need the access to the dataset of Keenan [7] to test our theory against null hypothesis and give a quantitative estimation on the probability of the existence of local void and the corrected H_0 after taking inhomogeneity into account.

8.2 Microscopic Universe

We show that a non-commutative spacetime theory can be constructed on top of Adler's "linear line element", and derive the associated action from the fermionization of the K-K ground state of the Polyakov action on a cylinder. The theory is shown to be holographic, and passes the astrophysical tests on the smearing effect and Lorentz invariance violation. The theory can also be regarded as the 4-D extension to the $U(\mathfrak{su}(2))$ model, and from there the generalized uncertainty principle is derived.

The theory is quite potent, and many aspects of the theory still remain unsolved. E.g., one may try to fix the Bekenstein-Hawking coefficient k inside Bekenstein's formula $S = kA/4$. We have also introduced kinematics of the theory only. The dynamics of the theory can be introduced through adding loop quantum gravity to the theory, or by adding back the K-K tower of the worldsheet excitation. Interestingly in loop quantum gravity [32], it has been argued that the length operator should be defined through Dirac operators. It remains curious whether our work can be served as a representation that can describe length, area and volume easily without introducing the spectral decomposition [26, 33].

doi:10.6342/NTU201603461

Appendix: List of Abbreviations

general relativity (GR)
standard model (SM)
supernovae (SNe)
cosmological microwave background (CMB)
local Hubble parameter (H_0)
mega-parsec (Mpc)
luminosity distance (D_L)
Milky Way (MW)
Monte Carlo (MC)
Friedmann–Robertson–Walker (FRW)
Lemaître-Tolman-Bondi (LTB)
section (sec.)
chapter (ch.)
equation (eq.)
equations (eqs.)
quantum mechanics(QM)
quantum field theory (QFT)
generalized uncertainty principle (GUP)
de Sitter (dS)
Anti de Sitter (AdS)
Kaluza-Klein (K-K)
Arnowitt-Deser-Misner (ADM)

Bibliography

[1] Antonio Enea Romano, Sergio Andrés Vallejo, “Directional dependence of the local estimation of H_0 and the nonperturbative effects of primordial curvature perturbations”, *Europhys. Lett.* **109, 3**, 39002 (2015).

[2] Antonio Enea Romano, Hsu-Wen Chiang and Pisin Chen, “A new method to determine large scale structure from the luminosity distance”, *Class. Quantum Grav.* **31**, 115008 (2014).

[3] Adam G. Riess *et al.*, “A 2.4% Determination of the Local Value of the Hubble Constant”, arxiv:1604.01424.

[4] Planck Collaboration, “Planck intermediate results. XLVI. Reduction of large-scale systematic effects in HFI polarization maps and estimation of the reionization optical depth”, arxiv:1605.02985.

[5] N. Suzuki *et al.*, “The *Hubble Space Telescope* Cluster Supernova Survey: V. Improving the Dark Energy Constraints Above z¿1 and Building an Early-Type-Hosted Supernova Sample”, *Astrophys. J.* **746**, 85 (2012).

[6] Adam G. Riess *et al.*, “A 3% Solution: Determination of the Hubble Constant with the Hubble Space Telescope and Wide Field Camera 3”, *Astrophys. J.* **730**, 119 (2011).

[7] R. C. Keenan *et al.*, “Evidence for a $\sim$300 Mpc Scale Under-density in the Local Galaxy Distribution”, *Astrophys. J.* **775**, 62 (2013).

[8] Krzysztof Bolejko *et al.*, “Anti-lensing: the bright side of voids”, *Phys. Rev. Lett.* **110**, 021302 (2013).

[9] H.-W. Chiang, Y.-C. Hu, P. Chen, “Quantization of Spacetime Based on Spacetime Interval Operator”, *Phys. Rev.* **D93**, 084043 (2016), [arXiv:1512.03157].

[10] David Mattingly, “Modern Tests of Lorentz Invariance”, *Living Rev. Relativity* **8**, 5 (2005), arxiv:gr-qc/0502097.

[11] Hartland S. Snyder, “Quantized Space-Time”, *Phys. Rev.* **71**, 38 (1947).

[12] Shahn Majid and Henri Ruegg, “Bicrossproduct structure of κ-Poincaré group and non-commutative geometry”, *Phys. Lett.* **B334**, 348 (1994), arxiv:hep-th/9405107.

[13] Jerzy Kowalski-Glikman and Sebastian Nowak, “Non-commutative space-time of Doubly Special Relativity theories”, *Int. J. Mod. Phys.* **D12**, 299 (2003), arxiv:hep-th/0204245.

[14] Jerzy Kowalski-Glikman, “Introduction to Doubly Special Relativity”, *Planck Scale Effects in Astrophysics and Cosmology* pp 131, Springer Berlin Heidelberg (2005), arxiv:hep-th/0405273.

[15] G. Amelino-Camelia, “Doubly-special relativity: first results and key open problems”, *Int. J. Mod. Phys.* **D11**, 1643 (2002), arxiv:gr-qc/0210063.

[16] Alain Connes and John Lott, “Particle models and noncommutative geometry”, *Nucl. Phys.* **B18**, 29 (1991), library of UMichigan.

[17] Alain Connes, “Gravity coupled with matter and the foundation of non commutative geometry”, *Commun. Math. Phys.* **182**, 155 (1996), arxiv:hep-th/9603053.

[18] Eliezer Batista and Shahn Majid, “Noncommutative Geometry Of Angular Momentum Space $U(\mathfrak{su}(2))$”, *J. Math. Phys.* **44**, 107 (2003), arxiv:hep-th/0205128.

[19] Laurent Freidel and Shahn Majid, “Noncommutative harmonic analysis, sampling theory and the Duflo map in 2+1 quantum gravity”, *Class. Quantum Grav.* **25**, 045006 (2008), arxiv:hep-th/0601004.

[20] Eliezer Batista and Shahn Majid, “Three dimensional quantum geometry and deformed symmetry”, *J. Math. Phys.* **50**, 052503 (2009), arxiv:0806.4121.

[21] Sergio Doplicher, Klaus Fredenhagen, and John E. Roberts, “The quantum structure of spacetime at the Planck scale and quantum fields”, *Commun. Math. Phys.* **172**, 187 (1995), arxiv:hep-th/0303037.

[22] Ronald J. Adler, “A quantum theory of distance along a curve”, Unpublished (2014), arxiv:1402.5921.

[23] Jungjai Lee, John J. Oh, and Hyun Seok Yang, “An Efficient Representation of Euclidean Gravity I”, *JHEP* **12**, 025 (2011), arxiv:1109.6644.

doi:10.6342/NTU201603461

[24] U. Carow-Watamura, M. Schlieker, M. Scholl and S. Watamura, “Tensor Representation of the Quantum Group $SL_q(2,\mathbb{C})$ and Quantum Minkowski Space”, *Z. Phys.* **C 48**, 159 (1990), Springer.

[25] Nathan Seiberg and Edward Witten, “String Theory and Noncommutative Geometry”, *JHEP* **09**, 032 (1999), arxiv:hep-th/9908142.

[26] T. Thiemann, “A length operator for canonical quantum gravity”, *J. Math. Phys.* **39**, 3372-3392 (1998), arxiv:gr-qc/9606092.

[27] M. Peskin and D. Schroeder, *Introduction to Quantum Field Theory*

[28] Sidney Coleman, “Quantum sine-Gordon equation as the massive Thirring model”, *Phys. Rev.* **D11**, 2088 (1975), Freie Universität Berlin.

[29] Edward Witten, “Non-Abelian Bosonization in Two Dimensions”, *Commun. Math. Phys.* **92**, 455-472 (1984), Project Euclid.

[30] Paul J. Steinhardt, “Baryons and baryonium in QCD$_2$”, *Nucl. Phys.* **B176**, 100-112 (1980).

[31] Francois Foucart, Evan O’Connor, Luke Roberts, Matthew D. Duez, Roland Haas, Lawrence E. Kidder, Christian D. Ott, Harald P. Pfeiffer, Mark A. Scheel, and Bela Szilagyi “Post-merger evolution of a neutron star-black hole binary with neutrino transport”, *Phys. Rev.* **D91**, 124021 (2015), arxiv:1502.04146.

[32] Carlo Rovelli, “Lorentzian Connes Distance, Spectral Graph Distance and Loop Gravity”, Unpublished (2014), arxiv:1408.3260.

[33] Eugenio Bianchi, “The length operator in Loop Quantum Gravity”, *Nucl. Phys.* **B807**, 591 (2009), arxiv:0806.4710.